NTNU – Trondheim
Norwegian University of
Science and Technology

Modelling of Gas Entrainment in Slugs through use of Simulations in StarCCM+ and Mechanistic Balance

Jørgen Nordbø

Chemical Engineering and Biotechnology
Submission date: June 2014
Supervisor: Martin Smedstad Foss, IKP
Co-supervisor: Jinsong Hua, Institutt for Energiteknikk

Norwegian University of Science and Technology
Department of Chemical Engineering

Abstract

Slug flow is a flow pattern existing at intermediate flow rates, or arising due to operating conditions or pipe topology. Typical slug flow is recognized by large gas bubbles flowing over a liquid film separated by liquid slug bodies with entrained gas bubbles covering the whole pipe diameter. The entrainment of gas requires an extra equation to be able to calculate the pressure drop of the flow. A good prediction of slug flows is needed in order to optimize the equipment sizing and operate multiphase transport pipelines in a best possible way.

In this study, a two-dimensional, transient channel setup of gas entrainment was simulated using the CFD package Star-CCM+. In order to enable the study of the entrainment of gas at the slug front, a moving reference frame with the propagation velocity of a Taylor bubble was applied. The simulations showed that all the parameters studied in the study; pipe inclination, bubble propagation velocity and liquid film height and velocity all revealed changes in the gas entrainment. The gas entrainment was found to be influenced by the turbulent kinetic energy in the liquid slug arising from the shear between the liquid slug and the liquid film. Furthermore, a mechanistic balance for horizontal pipes was solved to enable the usage of models using the momentum exchange as a parameter when calculating the liquid holdup. Two models considering the momentum exchange between the liquid film and the slug body were compared to other, more simple models. The best prediction model was found to be the model based on a dimensionless momentum transfer rate.

Both the simulations and the solving of a mechanistic balance for experimental values indicated that the momentum transfer rate at the slug front has an effect on the void fraction and gas entrainment. This effect may therefore be a good way to estimate the liquid holdup.

Sammendrag

Slugstrømning er et strømningsmønster som forekommer ved middels høye strømningsrater, eller grunnet driftsvilkår eller rørtopologi. Typisk slugstrømning kjennetegnes ved store gassbobler som strømmer over væskefilm, separert av store væskeansamling, med innblandete gassbobler, som fyller hele røret. Innblandingen av gassbobler gjør det nødvendig med en ekstra ligning for å kunne beregne trykkfall i strømningen. En god estimering av gassandelen i væskeansamlingen er nødvendig for å kunne designe utstyr riktig og for å kunne drifte transportrør best mulig.

I denne studien ble et 2D-oppsett av gassinnblanding simulert ved bruk av det kommersielle CFD programmet StarCCM+. For bedre å kunne studerer gassinnblandingen, ble et bevegelig koordinatsystem benyttet. Simuleringene viste at alle parameterene evaluert i studien; rørhelningen, boblenes propageringshastighet, væskefilmhastigheten og væskefilmhøyden, hadde påvirkning på gassinnblandingen. Gassinnblandingen ble vist å være relatert til den turbulente kinetiske energien i væskeslugen som oppstår grunnet skjæringskrefter mellom væskefilmen og slugfronten.

En mekanisk balanse for horisontale rør ble løst for å kunne sammenligne modeller som benytter seg av impulsoverføring som en parameter ved beregningen av væskemengden i slugen. To modeller som bruker denne parameteren ble sammenlignet med andre, enklere modeller. Den beste metoden viste seg å være metoden som benyttet seg av en dimensjonsløs impulsoverføringsrate.

Både simulering og resultater fra den mekaniske balansen viste at impulsoverføringsraten ved slugfronten har en påvirkning på væskemengden og gassinnblandingen. Denne parameteren kan derfor antas å være en god måte å beregne gassmengden i væskeansamlingen på.

Preface

This master thesis is the concluding work of a Master of Science in Chemical Engineering from the Norwegian University of Science and Technology (NTNU). The work has been preformed during the spring of 2014, under the guidance of Dr. Jinsong Hua. The thesis is submitted at the Department of Chemical Engineering at NTNU, but was done at the Institute of Energy Technology (IFE) at Kjeller.

Firstly, I would like to thank Jinsong for his kind guidance during the whole semester and for being patient when I was not. My thanks also go to Dr. Martin Foss for making it possible for me to write a master thesis on CFD and multiphase flow.

Furthermore, my parents, Øyvind and Elisabeth, deserve the deepest thanks for their good luck messages on examination days, motivational speeches and kind support these past six years. They, together with Rasmus, Preben, Bendik and Bastian, have made sure it always has been good to come home.

Lastly, I want to thank my fellow students at NTNU and TUM, without whom these past six years certainly would not have been such a blast.

I declare that this is an independent work according to the exam regulations of the Norwegian University of Science and Technology (NTNU).

Oslo, 16/6-2014
Place, date

Jørgen Nordbø
Signature

Contents

List of Tables

List of Figures

List of symbols

U, V	Velocity
u, u'	Velocity fluctuation
$\overline{u}$	Mean velocity
ϵ	Energy dissipation
ρ	Density
μ	Dynamic viscosity
ν	Kinematic viscosity
p	Pressure
$\mathbf{f}$	Force
σ	Surface tension coefficient
κ	Surface curvature
τ	Shear stress
C	Constant
k	Turbulent kinetic energy
l	Length; with subscript: length fraction
θ	Angle
Φ	Angle, flux, void fraction
Fr	Froude number
Re	Reynolds number
g	Gravitational acceleration
D, d	Diameter
A	Area
S	Circumference
f	Friction factor
L	Length
e	Energy
Q	Rate
Subscripts	
l, L	Liquid phase
g, G	Gas phase, gravity
b	Body, bubble

ST	Surface tension
i, j	Directional indicators
t	Turbulent, translation
T	Turbulent
r	Radial
f	Film, front
m, M	Mixture
s	Slug body
SL	Superficial liquid
SG	Superficial gas
d	Drift
h	Hydraulic
i	Interface
GS	Total entrained gas
Lf	Liquid film
Gb	Gas backflow
Ge	Gas entrainment
LS	liquid slug
TB	Taylor bubble
wb	Wall-bubble
wf	Wall-film
GB	Gas in bubble zone
LB	Liquid in bubble zone
u	Unit
nw	Near wake
$diss$	Dissipation
i	Impact

Superscript	
w	Wake zone
TB	Taylor bubble
$-$	Backflow
p	Plunging

Part 1

Introduction

1.1 Slug flow

Slug flow is a phenomenon encountered in many applications where multiphase flow is present. The different phases may be the same compound in different states, or two phases that are not miscible on a molecular level. Emergency cooling of nuclear reactors, boiling and condensation in liquid-vapour systems, geothermal production of steam, heat and mass transfer in chemical reactors and production of oil and gas are typical applications frequently experiencing slug flow.

The formation of slug in pipes may arise under different conditions, which have been summarized into three different cases [1] as listed below;

- **Hydrodynamic effects**
- **Terrain effects**.
- **Operating conditions**

Hydrodynamic effects include the slug formation due to a phenomenon

called Bernoulli suction, where small instabilities at the flow interface are allowed to grow resulting in the formation of liquid slugs. The terrain may affect the flow as changed pipe inclination and a local low-point in the pipe topology may choose an accumulation of liquid, as shown in Figure 1.1. A build up of pressure upstream of the liquid will then eventually cause the liquid to be transported further as a liquid slug, often referred to as severe slugging. Operating conditions as pipping pipes and start-up may also cause formation of slugs, before the flow is stabilized at normal conditions.

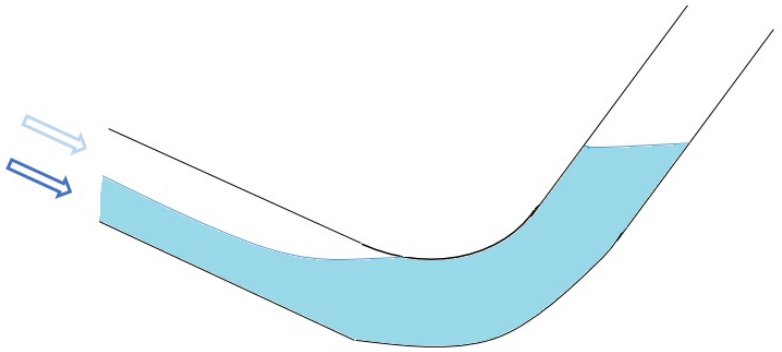

Figure 1.1: Severe slugging due to pipe topology

In horizontal pipes, slug flow is normally found at intermediate flow rates. Lower flow rates of both gas and liquids will be transported as stratified flow, but when increasing one, or both of the phase velocities, transitions to other flow regime will happen. Figure 1.2 shows a typical diagram with flow pattern normally present at the velocities in question. The flow pattern will also be dependent on the physical properties of the fluids and pipe geometry, shifting the boarder for transition to slug flow for the individual cases[2].

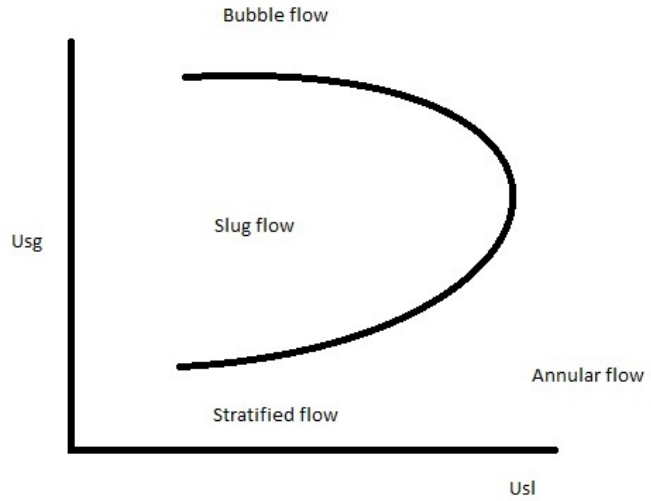

Figure 1.2: General flow regime structure for horizontal pipe

Under the right operating conditions, slug flow can be a regular sequences of liquid slugs separated by large gas bubbles flowing through the pipe, see Figure 1.3.

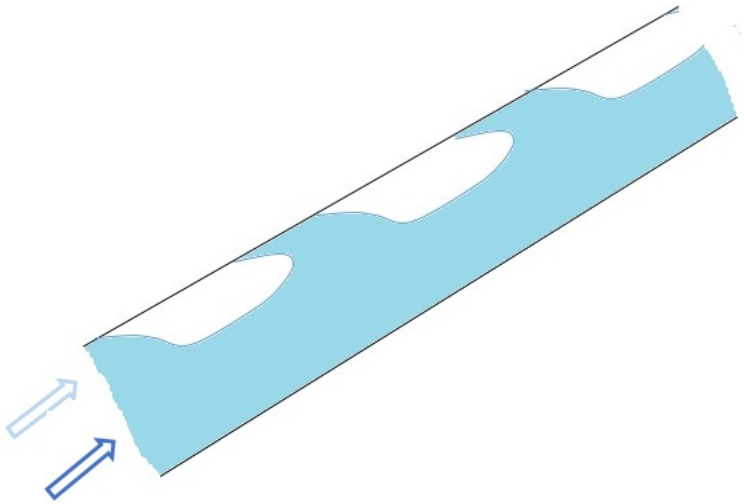

Figure 1.3: Stable slug flow

1.2 Studies of slug flow

Slug flow is one of the most complex flow patterns that can occur, making it difficult to study. A typical characteristic of slug flow is its inherent intermittence which can make the flow unstable even at constant flow rates of gas and liquid. The local velocity in slug flows will be different with the position in the flow. The liquid velocity of the liquid slug body will be higher than the liquid velocity in the film. This will cause a momentum exchange as the slug front overruns the liquid film. As a results, turbulence will be invoked in the slug body and entrainment of gas bubbles of multiple length scales may occur. Different mechanisms for gas entrainment are normally present, and the transportation of the gas bubbles in the liquid slug may be in both flow direction and opposite to it. The gas bubbles entrained will lower the liquid hold-up in the slug body, which then will change the pressure drop. Good estimation of the void fraction in the liquid

slug is therefore necessary in order to acquire good prediction of the flow conditions.

Many types of studies have been performed in order to understand the physical concepts relating to slug flow. Experiments used to quantify how the different physical properties as mixture and superficial velocities, pipe diameter, inclination and fluid properties have been studied by many authors over many years. Gregory et al. studied in 1978 [3] how the mixture velocity had an effect on the void fraction in the liquid slug body by measuring the void fraction in the slug, Nädler and Mewes (1995) [4] studied the effect of the liquid viscosity and Nuland et al. (1997) studied flow at different inclinations. Over the years the possibility to preform detailed studies on the physics in the liquid slugs have become possible. Wang et al (2012)[5] and Barnea et al. (2013)[6] studied the liquid slug body in more detail, evaluating the distribution of the bubbles in the liquid slug body. The experimental study of slug flow can be preformed in different ways. One is to study slugs when the slug flow is the stable flow pattern for the operation parameters chosen. Another is the study of a bubble travelling in liquid, measuring the bubble size and thereby understanding the gas entrainment into the liquid behind, as done by Abdullahi [1] .

Mechanistic models was used by Taitel and Dukler(1990) [7] to calculate the different parameters in the slug in order to predict the pressure drop. A general mechanistic model for slug flow in horizontal pipes have been presented and used, see e.g. Orell(2005)[8] and Al-Safran(2009)[9]. A more advanced model allowing for non-uniform void fraction in the slug body was presented by Brauner and Ullmann (2004) [10].

As the field of computational fluid dynamics (CFD) have grown over the last decades, CFD has also been used to study different features of slug flow. CFD makes it possible to in more detail study the physical processes happening when gas is entrained in the liquid slug. Therefore CFD simulations makes it possible to study how the entrained

gas bubbles affect the hydrodynamics in the liquid slug, as done by Yan and Che (2010) [11] or the transition between stratified flow and slug flow, as done by Höhne (2009) [12]. A way to reduce the computational need is to reduce the simulation from a 3D problem to a 2D setup. This will however change the accuracy of the simulation, and Mo et al. (2013) [13] proposed a Quasi-3D setup in order to have higher accuracy but lower computational costs than a full 3D simulation.

1.3 This work

The study of slug flow and the gas entrainment is difficult due to the complex physics and multiple parameters influencing them. In this report, first a CFD simulations of a slug front will be analysed with special focus on the parameters effecting the gas entrainment at the slug front. Due to all the assumptions done when simulating a slug front, the simulation results are expected to show general trends and the importance of the different factors influencing the entrainment.

Furthermore a mechanistic model for horizontal pipes will be solved in order to study the slug flow in more detail than a simple prediction model. The mechanistic model prediction models use multiple of the velocities in a slug to calculate the void fraction and make it possible to study the momentum transfer rate between the liquid film and the slug body at the slug front.

Part 2

Background

2.1 Unit Cell

For studies of slug flow the Unit Cell (UC) model is a common concept [14]. This model serves to understand the behaviour of slug units consisting of the smallest repetitive unit of the slug flow. The unit is divided into two smaller zones, one for the large gas bubble, and one for the liquid slug body. The UC model can be said to study a characteristic unit of the liquid slug and one corresponding large bubble.

The UC model makes some assumptions regarding the slug flow. The first assumption is that the flow would be steady at an existing frame velocity. The second assumption is that the flow in the long bubbles and the liquids slugs is fully developed. For a fully developed flow, the values of the flow will not change in longitudinal direction as long as it is not going from one zone to another. This assumption indicates that the longitudinal position will not effect the phase fraction, as long as it is in the same part of the slug, either the bubble or the liquid slug.

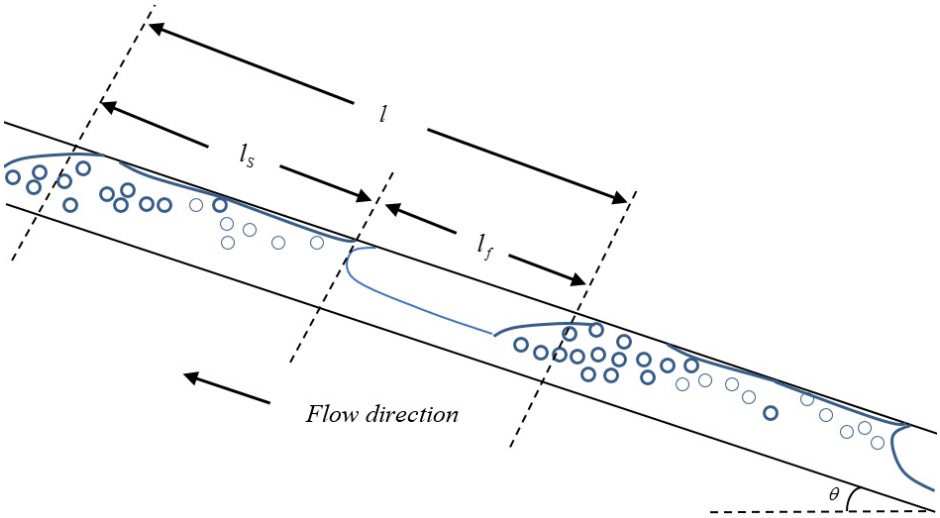

Figure 2.1: Unit cell concept for slug flow

The liquid in front of the elongated bubble will be accelerated when the bubble nose approaches and then be drained as a film under or around the elongated bubble for horizontal or vertical pipes respectively.

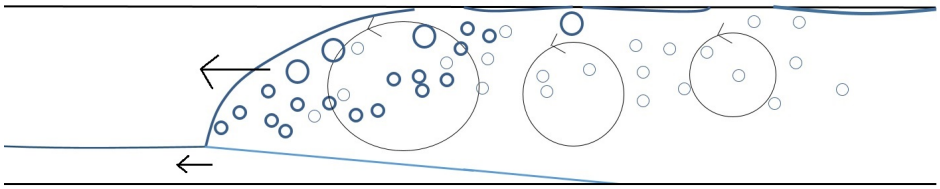

Figure 2.2: Film layer entering liquid slug causing turbulence

At the end of the Taylor bubble there will be a hydraulic jump. Here the liquid film will be overrun by a liquid slug increasing the water depth for a classic hydraulic jump and change the liquid velocity. Effectively, the film will enter the liquid slug as a jet. The momentum

of the film and the liquid slug body will determine the height of the jump and how the velocity field develops behind the slug front. A classic hydraulic jump will show an increase of liquid depth, reduction of energy and velocity downstream. From the conservation equations for mass and momentum, it is possible to derive jump conditions for one-phase flow. For two phase flow, mixing will occur which will lead to a new unknown parameter; the entrainment of one phase into the other. The calculation of the hydraulic jump requires closure strategies for the calculation of the entrainment. One closure hypothesis made by Holland et al.[15] assumes that turbulence in a strong, internal hydraulic jump gets its energy from the energy dissipation in the jump. This energy dissipation will be bound by how much turbulence one can have in separated flow.

2.1.1 Taylor bubble

The shape of a Taylor bubble(TB) can be divided into four different parts; nose, body, jump and tail, see Figure 2.3.

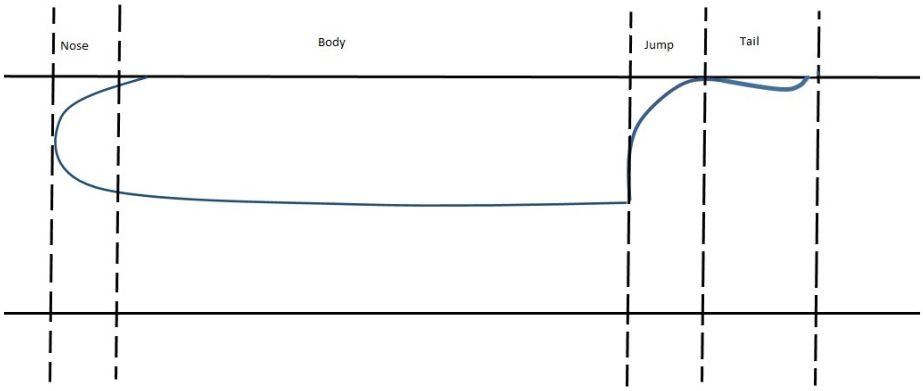

Figure 2.3: Different sections of a Taylor bubble

For low liquid velocities the jump does not fill the whole pipe and a tail is formed (Fr $<$ 1). The tail is observed to get thinner and shorter for increasing liquid velocities. For high velocities the tail will disappear and entrainment of bubbles in the wake of the long bubble is observed (Fr $>$ 2). Tails may be observed at liquid velocities below 0.8 m/s, and will be dependent on the bubble length if the Fr number is between 1 and 3.[16]

$$Fr_U = \frac{U}{\sqrt{gD}} \tag{2.1}$$

2.2 Turbulence

Turbulence is a flow phenomenon that is hard to describe precisely, but it is often explained by some characteristic, describing the nature of turbulence. A turbulent flow will typically have some features that characterize its turbulence; irregularity, randomness, dissipation and vorticity movement in all spacial dimensions. Turbulent flow exists only at high Reynolds numbers, it is a continuum phenomenon and a flow property, not a fluid property. A turbulent flow can however not be completely random, since it always has to fulfil the continuum equations. The occurrence of turbulence is large and turbulence can be found from places in ocean currents and rivers to chemical reactors, heat exchangers and fluid transport pipes. Since turbulence is dissipative it will decay in time if no contribution to sustain it is present. [17]

To make the description of turbulence easier, the turbulence is often tested for isentropy and homogeneity. A turbulent flow is said to be isentropic when all the statistical properties and all turbulent scales are independent of direction in the flow. Homogeneous turbulence is the case when the different velocity fluctuations and derivatives are independent of position, but still dependent on direction. [18]

The dissipation of turbulent flows give rise to a turbulent eddy energy cascade. Here the first induced turbulent eddies effect the surroundings, giving rise to smaller vortices. The turbulent energy first put into the cascade will in the end, end up as energy in form of heat when the cascade reaches vortices at the size of Kolmogorovs turbulent length scales, which again are dependent on the respective fluid properties.

For multiphase cases, shear layers between the phases will occur and induce turbulence. The phases will be mixed in the turbulent layer, and fluid properties will be diffused if the phases are miscible. For phases immiscible on a molecular level, entrainment of the phases in each other will occur, and separation of the phase i.e. due to gravity may occur. The flow properties will be diffused and transported between the phases, making the turbulent conditions in the different phases depending on the total flow.

2.3 Effect of physical parameters

The effect of how physical properties of the flow and fluids effect the gas entrainment process has been subject to many studies over the last decades. These properties effect effect the entrainment in different ways, but as the change of fluid often includes changing more than one parameter (i.e. density, viscosity and surface tension) the contribution of the individual contribution may sometimes be difficult to quantify.

Nuland et al. [19] found a strong liquid viscosity dependency for the void fraction of slug flow with a possible explanation being the complex entrainment mechanisms occurring at the slug front, see Section 2.4.1. This complex dependency makes it hard to quantify the liquid viscosity effect in simple dimensionless numbers (i.e. Weber number). The surface tension and gas density have shown to be of

large influence on the void fraction [20], and a high gas density makes the slug flow structure very complex [19].

Nädler [4] compared results with different liquid viscosities and found that the liquid viscosity had little effect on the liquid film holdup under the TB. The liquid viscosity was found to increase the void fraction in the liquid slug when increased. Increased superficial liquid velocity was found to increase the liquid holdup. The effect of the liquid viscosity was found to decrease with increasing superficial liquid velocities. Considering only the liquid slug section, a decrease in liquid holdup was found for increasing surface tension. With the observed decrease of liquid holdup when increased liquid viscosity, a increase of the liquid film was also observed. By continuity the gas velocity in the TB must be higher for higher liquid holdups.

2.3.1 Pipe geometry

Changing the pipe diameter has been found to change the lower threshold velocity above which gas is entrained in the liquid slug body. The diameter has also been found to give a more rapid rise in the void fraction when increasing the mixture velocity for larger pipe diameters.[20]

Declining the pipe slightly has shown a decrease of the void fraction compared to horizontal flow. This might be a result of the decrease of the TB velocity (due to lower relative drift of the TB) yielding a lower relative velocity between the slug front and the film.[20]

Nuland et al. [19] used the concept from the flow model OLGA, see Section 2.5.4, to adjust the effect of pipe inclination for calculation of the void fraction. For similar flow condition, a horizontal pipe would give stratified flow as the stable flow, whilst inclined pipes would show slug flow. At higher inclination (above 60°) the different flow patterns were hard to separate and to identify asslug, plug or annular flow.

Abed et al. [21] studied gas-liquid slug flow in a 30° upward inclined 4 meter long test section by evaluating the pressure in the pipe. The pressure drop was found to increase with increased superficial velocities. Higher pressures were found for increased liquid viscosity.

2.4 Entrainment of gas bubbles

2.4.1 Physical description of entrainment mechanisms

The different physical mechanisms for entrainment of gas bubbles have been studied and described by many authors, both experimentally and by simulations. Nuland et al [19] described small bubbles being entrapped at the base of the hydraulic jump where the slug overruns the slower moving liquid in the liquid film. Vortices in the upper part, above the liquid film height, were observed. At the front of the liquid slug breaking waves entraining larger bubbles were observed. The large bubbles would be positioned at the wall and move downstream into the slug due to lower velocity at the walls. The small bubbles would be moved into the slug due to a relative lower velocity where they will be entrained and gradually distributed over the whole pipe section. Some of the bubbles would be moved away from the wall due to lift forces arising from the wall shear stresses.

In the simulations made by Taha and Cui [22] a highly agitated mixing bubble wake zone was observed due to impingement of the wall jet inducing circulation in the pipe. Depending on thinverse viscosity dimensionless number, N_f, the wake take different patterns. [22]

2.4.2 Distribution of entrained gas bubbles

Wang et al. (2012) [5] studied how the entrained bubbles would be effected by the flow in the slug, and how the void fractions would be distributed in horizontal pipes by recording the void fraction at different positions in the pipe. From observations of the experiments it was found that the dispersed bubbles would congregate and coalesce into larger bubble when situated in the middle or upper part of the pipe. Further downstream in the pipe this effect make a transition to plug flow or stratified flow. It was also observed that most of the gas entrainment happened at the impingement point at the intersection between the mixture layer and the liquid film. After the impingement point the bubbles were broken into smaller bubbles in a layer with high shear stresses. Many of these small bubbles would advect into a turbulent shear layer at the lower part of the pipe. The recirculation layer was observed to be a high turbulent bubble flow with large eddies, reverse flow at the top of the pipe and splashes. Close to the liquid slug front peaks of void fraction distribution were found correspondent to entrainment happing at the impingement point. These peaks disappeared further downstream indicating that the turbulent layer increased while the turbulent intensity decreased.

The effect of changing the Reynolds and Froude film numbers were found to decrease the gas entrainment for decreasing numbers. The peaks of the void fraction would also decrease with decreased Froude numbers, as well as a decrease of the mixing region length, letting the flow to become fully developed at an earlier stage. Peaks of the radial distribution of the void fraction and bubble frequency were found in the mixing region turbulent shear layer.

Barnea et al. (2013) [6] performed a three dimensional experimental study of the void fraction in liquid slug. A wire mesh sensor was used for all inclinations. At the test facility a pipe length of 10 m with an internal diameter of 54 mm was used, the fluids used were air and water. In order to reduce end effects and to let the slug

stabilize, the measuring station was positioned 8 m from the inlet. During the experiments it was observed that for low mixture velocities, $U_m < 0.4m/s$ and slightly inclined pipe, no entrained bubbles could be seen. The pipe inclinations ranged from 2° to vertical, with different superficial velocities for all inclinations considered.

The elongated bubble's tail served as the reference for the determination of the spatial distribution of the slug. The identification of the elongated bubbles was done by considering a threshold for the void fraction, typically 0.9. The bubble length was considered to be as long as the void fraction was above this threshold. Knowing the position of the end of the elongated bubble, made it possible to use this as a reference for the study of the void fraction by considering a distance into the slug from the end of the bubble.

In order to study the spatial distribution the void fraction of an ensemble of cases were averaged. This averaged data was further average at 8 different horizontal(longitudinal) levels with equal distance between them for the cases with inclined pipes. For the lowest levels, very little dependency on the inclination and velocities was found. For the higher levels high void fraction was observed near the end of the elongated bubble, decaying fast with distance into the liquid slug. A minimum of the void fraction was found at distances into the slug $2 < x/D < 6$. The changing inclination was found to increased the region where dispersed bubbles were found. From low mixture velocities and inclination where the void fraction disappeared fast, to higher inclinations where the void fractions for all levels were found to increase. For higher inclinations the void fraction spread more out on more levels, than at low inclinatiosn where the void fraction was mainly found at the top of the pipe.

For vertical pipes, the longitudinal levels did not provide maximum information due to the axial symmetry of the flow. A new approach using a ring with smaller and smaller diameter was therefore used to study the spatial distribution for vertical flow. The void fraction was found to be low along the pipe walls and high in the center of the

pipe. It decreased from high values near the elongated bubble to a minimum at $x/D = 3$, after where it started to slowly increase to a nearly constant level.

Considering the overall void fraction it was found to be very low for low mixture velocities at low inclinations. Increasing the mixture velocity resulted in an increased void fraction. Small bubbles were found dispersed in the liquid slug even at very low mixture velocities at high inclinations. Keeping the mixture velocity constant varying the superficial velocities showed that higher superficial gas velocities give slightly increased void fraction.

2.4.3 Entrained bubbles effect on hydrodynamics

Yan and Che presented in 2010 [11] a paper evaluating the effects of dispersed bubbles on the hydrodynamics of vertical slug flow studied numerically. They evaluated the effect the dispersed bubbles have on the physics in the slug, since the bubbles not only will take up volume, but also interact with surrounding the fluid.

The presence of dispersed small bubbles in the film zone and the region in front of the Taylor bubble did not influence the physics in these parts significantly. In the Taylor bubble wake (TBW) zone in the liquid slug there is an intensive recirculation. Hence, the small dispersed bubbles are not distributed uniformly. In the recirculation region there will also be produced centrifugal forces. Due to the large density difference and the interactions between the bubbles and the surrounding fluid, the flow field will be effected. The coalescence of small bubbles into larger bubbles, was not considered due to the numerical method used. The fluids where evaluated as three phases; gas, liquid, and bubbles smaller than one grid cell. The small bubbles were therefore a fraction of the field, and not separated clear bubbles where it is possible to track the surface. The centrifugal forces in the

TBW and the heterogeneous distribution of the small bubbles were reported to effect the radial velocity profile sharper with increasing fraction of small bubbles. The presence of small bubbles was also seen as an increase in wall shear stress and the mass transfer coefficient. This was explained as a results of increasing fluctuations in the wake region.

Mechanistic considerations of gas entrainment mechanisms

Studying the different mechanisms resulting in gas entrainment has also been used as a basis of finding new parameters telling more about the slug. Following here is how different papers used the knowledge of the entrainment mechanisms to approximate the total gas entrainment in the liquid slug.

In 1989, Andreussi and Bendiksen [20] argued that due to the vortices in the liquid slug body, the gas entrainment would be dependent on multiple mechanisms, all contributing to the void fraction of the slug body. Two different mechanisms were evaluated and are explained in the following. The first mechanism is the gas bubble production rate into the slug, Q_1, whilst the second is the back-flow rate of small bubbles into the Taylor bubble, Q_2. The net gas entrainment rate at the slug front, Q_3 would hence be a function of these two, but at the same time also effected by the change of the volume of the Taylor bubble in front of the slug, see Equations 2.2 to 2.4

$$Q_1 = C_1 A \left[(1 - \epsilon_B) (U_B - U_{Lf}) - U'_{Mf} \right] \tag{2.2}$$

$$Q_2 = C_2 A \epsilon_s U_{G0} \tag{2.3}$$

$$Q_3 = A \epsilon_s (U_B - U_{Gs}) + \Delta Q_f \tag{2.4}$$

The gas bubble production rate, Equation 2.2, takes three different effects into account. It increases with both increasing relative slug and film velocities and it increases with increasing film height $(1 - \epsilon_B)$. The backflow rate, Equation 2.3, was assumed proportional to both the drift velocity of the entrained bubbles, U_{G0} and the void fraction in the slug. The net entrainment was based on continuity, with U_{Gs} being the average velocity of the gas in the slug, and ΔQ the possible contribution from droplets entrained in the liquid film. This last contribution was considered to be without any effect and thus neglected.

Skartlien et al. (2012) [23] studied the gas entrainment in a hydraulic jump when the subcritical flow filled the whole pipe, developing parameters not considering the liquid viscosity.

The gas entrainment mechanism was divided into three mechanisms. One mechanism for the entrainment due to liquid plunging into the liquid layer upstream, one for the entrapment of liquid at the base of the hydraulic jump and one for the leakage of gas through the front, Φ_p, Φ^- and Φ_f respectively. The turbulence kinetic energy and the large-scale recirculation downstream of the jump were considered to be important parameters effecting Φ_p and Φ^-.

$$\Phi = \Phi_p - \Phi^- + \Phi_f \tag{2.5}$$

The production rate of the turbulent kinetic energy was found to be a function of the difference in work between the jumps in pressure and velocity and the increase in gravitational potential energy, $\Delta \mathrm{E}_e$, and the work due to wall friction, $\Delta \mathrm{E}_0$. The turbulent production was then compared to a typical equation for turbulent energy dissipation. Based on this comparison, the turbulent kinetic energy was approximated as

$$k \approx \left[\frac{1}{C_\mu} \frac{L_{\text{mix}}}{L_{\text{diss}}} \frac{(\Delta \text{E}_e + \Delta \text{E}_0)}{\rho_{mix} A} \right]^{2/3} \tag{2.6}$$

The physical dissipation and mixture lengths were approximated by simple correlations evaluating the cross section area of the front of the hydraulic jump.

Liquid moving upstream towards the front of the jump will be responsible for the plunging entrainment mechanism. The circulation in the mixing zone downstream of the jump arises due to the fact that the liquid film upstream of the jump undercuts the slower moving subcritical liquid at the jump. Some the faster moving liquid is forced upwards in the subcritical part, and will circulate towards the front of the jump. The circulation combined with the turbulent kinetic energy will cause a dynamic pressure, and when the dynamic pressure is large enough, fluid expulsion can be expected. The circulation velocity can be approximated by the incoming film velocity, or be estimated by evaluating mass conservation for a cross-section with liquid moving downstream and upstream. The plunging entrainment was given the form

$$\Phi_p = C_p \Phi_{ls} \left(\frac{V_i}{V_0} \right)^n \tag{2.7}$$

using the liquid jet velocity, Φ_{ls}, the impact velocity, V_i, $n \approx 1.7$, and the normalizing velocity, $V_0 = \sqrt{g d_c}$. The $d_c = 0.2D$ is the diameter of the vertical jet and C_p is a proportionality constant. The impact velocity was approximated using the film velocity, the ejection velocity relative to the front and some potential energy consideration.

The backflow of entrained gas to the upstream gas pocket was considered to consist of one advection part and one turbulent diffusion part. Ignoring mass and lift effect and a possible energy threshold

for bubbles to break through the liquid front interface, and combining the advection and diffusion velocity terms to one, V_{da}^{+}, the total backflow flux was given by

$$\Phi^{-} = A_s V_{da}^{+} \alpha_{\text{mix}} \tag{2.8}$$

For the gas entrapment happening at the base of the hydraulic jump, Skartlien et al. adopted an earlier tested relationship for the gas entrainment flux, Φ_f,

$$\Phi_f = C_f S_i \frac{V_f^3}{g} \tag{2.9}$$

Earlier velocity onset threshold was ignored by Skartlien et al., but reported to be 1 m/s.

2.5 Void fraction estimations

2.5.1 Gregory 1978

Gregory et al.(1978)[3] studied the void fraction in slugs as a function of the mixture velocity. An empirical equation was presented, see Equation 2.10.

$$H_{ls} = \frac{1}{1 + \left(\frac{U_M}{8.66}\right)^{1.39}} \tag{2.10}$$

Due to the simplicity of the proposed equation, effect of diameter and fluid properties were not included.

2.5.2 Andreussi and Bendiksen 1989

The different mechanisms presented by Andreussi and Bendiksen [20], see Section 2.4.3, together with different mechanistic and physical approximations, gave rise to the expression in Equation 2.11, relating the void fraction to a threshold velocity, U_{Mf}. For velocities lower than U_{Mf}, the liquid film is immersed into the liquid slug without production of bubbles, and the mixture velocity, U_M.

$$\epsilon_s = \frac{U_M - U_{Mf}}{(\beta U_M + U_{M0})^m} \tag{2.11}$$

Evaluating experimental values, the different terms in Equation 2.11 as

$$U_{Mf}^{\infty} = \frac{U'_{Mf}}{C_0 - 1} = 2.60 \left[1 - \left(\frac{D_0}{D}\right)^2\right] \sqrt{gD} \tag{2.12}$$

$$U_{M0} = \frac{240}{C_0} \sqrt{\Sigma} \left(1 - \frac{1}{3}\sin\phi\right) \left(\frac{g\sigma\Delta\rho}{\rho_l^2}\right)^{1/4} + \frac{U_0}{C_0 - 1} \tag{2.13}$$

2.5.3 Nädler 1994

Nädler and Mewes [4] observed that an increase in superficial gas velocity lead to increased gas entrainment and decreased liquid film. The length of the TB was also observed to increase. When only considering the slug section, the holdup was found to decrease with increasing mixture velocities. The gas entrainment rate was found to be approximately proportional to relative velocities between the slug front and average gas velocity in TB, and between the slug front and the average liquid film velocity.

2.5.4 Nuland 1997

Considering pipe inclinations from 10° to 60°, Nuland et al. [19] tested how combining void fraction estimations for horizontal and vertical pipes would predict the void fractions for inclined pipes.

$$\epsilon_s(\alpha) = \epsilon_{sv} \cos\left(\alpha^2\right) + \epsilon_{sh} \sin\left(\alpha^2\right) \tag{2.14}$$

The correlation used for horizontal and vertical flow were as given in Equations 2.15 and 2.18, respectively.

$$\epsilon_{sh} = C_s \left(|U_{sl} + U_{sg}| - U_{ss}\right) \tag{2.15}$$

if $U_m > U_{ss}$.

$$U_{ss} = 2.57\sqrt{gD}\left(1 + 1.5\cos\left(\alpha\right)\text{sign}(\cos(\alpha))\right) \tag{2.16}$$

$$C_s = 0.15 + 0.001\rho_g \tag{2.17}$$

If $U_m < U_{ss}$ the horizontal entrainment was set to zero.

$$\epsilon_{sv} = \frac{0.3 + U_{sl} + U_{sg}}{C + U_{sl} + U_{sg}} \tag{2.18}$$

$$C = \frac{2.2}{1 + 0.02\rho_g} + 2U_{sl} \tag{2.19}$$

The general trends were found to be reproduced when testing the model for a new data set with an other fluid than the one used as basis for the equations. However, systematic deviation from the computed values were found.

2.5.5 Abdul-Majeed 2000

Abdul-Majeed presented in 2000 [24] a model based on a collection of different experimental data sets. Evaluating earlier models, it was commented that all the models considered assumed that the liquid slug holdup was a function of mixture velocity, and did not consider the different liquid and gas velocities. The dataset, considering seven different sources, contained 435 points, of which three were eliminated due to high gas velocities that would assumable lie in the annular flow region, and nine due to lower holdups than a stable liquid slug would contain, resulting in a dataset of 423 points. The dataset covered diameter from 2.58 cm to 17.145 cm, different types of fluid mixes, and three studies with different angels, ranging from -10 to 9 degrees. See Abdul-Majeed [24] for specific details.

The study of the data set concluded that the liquid slug holdup is only slightly affected by the diameter and surface tension. A general trend for the liquid slug holdup was presented, see Equation 2.20.

$$H_{LLS} = (1.009 - CV_M)\, A \tag{2.20}$$

where

$$C = 0.006 + 1.3377\, \frac{\mu_G}{\mu_L} \tag{2.21}$$

The C in Equation 2.21 accounts for the effect of increased void fraction for increased liquid viscosities, an effect referred to be independent of inclination by intuition.

The effect of the inclination on the holdup was accounted for by A in equation 2.20. The effect was found the differ for downwards and horizontal pipes compared to an upward inclined pipe. Based on this, A was given as in Equation 2.22.

$$A = \begin{cases} 1.0 & \text{for } \phi \leq 0 \\ 1.0 - \sin(\phi) & \text{for } \phi > 0 \end{cases} \tag{2.22}$$

The study showed that the predicted values for liquid slug holdup fitted with 10% of the measured data.

2.5.6 Zhang 2003

In 2003, Zhang et al. [25] considered the turbulent kinetic energy in the flow to break bubbles if this is stronger than the force making sure the bubble stay a bubble(the bubbles are over a critical value). The void fraction of a liquid is the amount of gas the slug can hold. Since the TKE is responsible for breaking droplets the void fraction will therefore be dependent on the turbulent intensity of the liquid phase.

It is possible to set up a balance between the total surface free energy and the turbulent kinetic energy in the liquid slug.

$$E_T = C_e E_s \tag{2.23}$$

Where E_T is defined as in 4.43, E_s as in Equation 4.46 and C_e as in Equation 2.24 below.

$$C_e = \frac{2.5 - |\sin\theta|}{2} \tag{2.24}$$

The liquid holdup in the liquid slug body was then calculated as

$$H_{Ls} = \frac{1}{1 + \frac{T_{sm}}{3.16[(\rho_L - \rho_g)g\sigma]^{1/2}}} \tag{2.25}$$

with T_{sm} being defined as

$$T_{sm} = \frac{1}{C_e}\left[\frac{f_s}{2}\rho_s U_m^2 + \frac{d}{4}\frac{\rho_L H_{Lf}\left(U_t - U_f\right)\left(U_m - U_f\right)}{l_s}\right] \tag{2.26}$$

The prediction of the model was tested for pipes with inclination from horizontal to vertical. The model was shown to predict the general trends good, but had some difficulties picking up the local scatter for different runs.

2.5.7 Al-Safran 2009

Al-Safran [9] presented in 2009 a model for calculation of liquid slug holdups. The holdup was related to a new parameter introduced as the dimensionless momentum transfer rate. This parameter was developed to represent the momentum exchange from the liquid slug body need to accelerate the slower moving liquid film. Using the liquid flux into the front of the slug, see Equation 2.27, and the superficial liquid momentum, see Equation 2.29, the momentum transfer rate was established as a mechanistic parameter. The momentum transfer rate would therefore be a function of multiple parameters, fluid properties, operational and geometric parameters when solved mechanistic, and will therefore be able to account for the holdup dependence of these parameters.

$$\dot{m_L} = \rho_L A_p H_f \left(U_t - U_f\right) \tag{2.27}$$

$$\text{Momentum rate liquid film} = \rho_L A_p H_f \left(U_t - U_f\right)\left(U_m - U_f\right) \tag{2.28}$$

$$\text{Momentum rate superficial liquid in slug} = \rho_l A_p U_{sl}^2 \tag{2.29}$$

$$\theta = \frac{\rho_L A_p H_f \left(U_t - U_f\right)\left(U_m - U_f\right)}{\rho_l A_p U_{sl}^2} \tag{2.30}$$

After considering a data bank, Al-Safran found the correlation to be better when using U_m as denominator instead of U_{sl}. The final momentum transfer rate is therefore as given in Equation 2.31

$$\Theta = \frac{H_f \left(U_t - U_f\right)\left(U_m - U_f\right)}{U_m^2} \tag{2.31}$$

A mechanistic model was used to study how the liquid slug holdup would vary with the dimensionless momentum transfer rate. The model was implicit and a starting value provided by the correlation of Gregory et al. was used as an initial value for the iteration process. When considering measured values of liquid holdup from different experiments compared to the momentum transfer rate, a non-linear correlation was discovered. The holdup was reported to be directly proportional with the transfer rate for low values, before the relationship turned over to be constant. A possible explanation of the relationship between the liquid slug holdup and the momentum transfer rate was proposed to be that an increase of the momentum transfer rate would mean an increase of liquid flux into the slug and therefore increasing the holdup. The effect of the increase in mixture velocity was seen to decrease the momentum transfer rate, since it can be found as a squared property in the denominator. Al-Safran found this effect to correspond to the findings of other authors. The momentum transfer rate is also directly proportional to the liquid film holdup, H_f. The liquid slug holdup will therefore increase with increasing liquid film holdup.

Regression analysis of the data considering liquid holdups in the slug versus the dimensionless momentum transfer rate gave the correlation given in Equation 2.32 below.

$$H_{LS} = 1.05 - \frac{0.0417}{\Theta - 0.123} \tag{2.32}$$

Part 3

Simulation of gas entrainment at slug front

3.1 Governing equations

The Navier-Stokes equations (NSE) describes the motion of fluids and arises by applying Newtons second law to fluid motion. The NSE is commonly used in computational fluid dynamics (CFD) calculations.

The general NSE for incompressible flow with constant viscosity is shown in Equation 3.1 and represents how the momentum changes when influence by body forces.

$$\rho\frac{\partial \mathbf{U}}{\partial t} + \rho(\mathbf{U}\cdot\nabla)\mathbf{U} = -\nabla p + \mathbf{f}_b + \mu(\nabla^2\mathbf{U}) \tag{3.1}$$

Here $\mathbf{U}$ is the velocity field and ρ the density. p is the pressure and μ is the dynamic viscosity. $\mathbf{f_b}$ represents the body forces acting on the fluid, including gravity and surface forces.

The physical conservation of mass in fluid flows is often expressed in terms of the continuity equation, Equation 3.2.

$$\frac{\partial \rho}{\partial t} + (\nabla \cdot \rho \mathbf{U}) = 0 \tag{3.2}$$

If the flow is incompressible, the density is constant and the continuity equations becomes Equation 3.3.

$$\nabla \cdot \mathbf{U} = 0 \tag{3.3}$$

The symbols used in Equations 3.2 and 3.3 are the same as those used in Equations 3.1. [26]

3.2 Multiphase flow

3.2.1 Interface modelling

For the calculation of two-phase flow a strategy has to be chosen on how to calculate the transport and distribution. When using the NSE as a model for two-phase flow, there is two main options. The first one is solving the NSE for each of the discrete phases and then coupling the fields together through the interface boundary. This method is often referred to interface-tracking method on Lagrangian grids. The other option is to solve the NSE for the whole flow field, also known as an one-fluid model using Eulerian grids. The interface is captured using additional equations, so-called closure laws.

Interface tracking
By the use of a Lagrangian method each phase are dedicated one mesh and the NSE is solved for each of the phases separately before the interface is calculated where the two different meshes meet and the different field are connected. The meshes will move with the phase and have to generate for each time step. [27] Interface tracking methods can be difficult to implement as they need additional equations for the mesh movement which can be hard to find [28].

Interface capturing
When using an Eulerian grid, where the mesh is fixed and the same for both phases, it is only necessary to solve the NSE one time for the whole domain. In Eulerian methods it is therefore important to implement functions that can show where the interface between the two phases is. Methods commonly used for one-fluid methods is the Volume of Fluid (VOF) method and the Level Set (LS) method. The VOF method was used in the following simulation and is explained further in Section 3.2.2.

The interface tracking approach has a higher accuracy than the interface capture approach, but at the cost of higher calculation cost and time[29]. An other advantage with the interface-tracking method is that coalescence will not occur unless specific merge conditions are implemented, while interface-capturing methods will coalesce bubbles automatically[30].

A combination of Interface Tracking and Interface Capturing methods have also been used[28]. Here a fixed grid was used described the fluid motion, while a second grid was used to track the interface. The second grid had a lower dimension than that used for calculation the fluid motion.

3.2.2 Volume of Fluid Method

In the Volume of Fluid (VOF) method the interface is captured by using a scalar function F which is transported in the domain by a convection equation as seen in Equation 3.4, which is written for a two dimension problem[31].

$$\frac{\partial \alpha}{\partial t} + u\frac{\partial \alpha}{\partial x} + v\frac{\partial \alpha}{\partial y} = 0 \tag{3.4}$$

The value of α vary between 0 and 1 depending on the fraction of the different phases in one cell. If the cell only contains one phase α is 0 and if it is only containing the other phase α is 1. All values between, indicate that both phases are present in the cell, and that the cell therefore contains an interface between the two phases.

$$\alpha = \begin{cases} 0 & \text{, in fluid 1} \\ 0 < \alpha < 1 & \text{, at the interface} \\ 1 & \text{, in fluid 2} \end{cases} \tag{3.5}$$

The VOF method does not give the structure of the interface, but only the position of it[32].

An advantage with the VOF method is capability of solving problems with significant topology changes, but a drawback is the is smears out numerically [28].

Dijkhuizen et al.(2007) stated that the use of VOF for calculating air bubbles in water to be difficult due to the simultaneous large differences in density and surface tension[33].

The VOF model is included in the flow simulation by effecting the surface tension force in the body forces term.

$$\mathbf{f}_b = \mathbf{f}_{ST} + \mathbf{f}_g \tag{3.6}$$

where the surface tension force is calculated as

$$\mathbf{f}_{ST} = \sigma\kappa\nabla\alpha \tag{3.7}$$

σ is the surface tension coefficient, and κ is the surface curvature defined as

$$\kappa = \nabla \cdot \mathbf{n} \quad \text{with} \quad \mathbf{n} = \frac{\nabla\alpha}{|\alpha|} \tag{3.8}$$

3.3 Turbulence

3.3.1 Turbulence modelling

When modelling turbulence, there exist three different main approaches; Direct Numerical Simulation(DNS), Large-Eddy Simulation(LES) and Reynolds Average Navier Stokes (RANS). When using RANS, the Navier-Stokes equation (NSE) are averaged and the flow will therefore not show any typical signs of turbulence. LES uses an approach that averages the NSE based on volume. Eddies over a certain size are solved numerically, whilst the rest is modelled. DNS solves all equations for the length and time scales of the turbulence, making this the approach with the highest demand for simulation power and storage space.

The RANS equations uses time averaging and then try to model the fluctuations. Every parameter in a mean value and a fluctuation, as shown in Equation 3.9

$$u = \overline{U} + u' \tag{3.9}$$

During the averaging, a set of rules are applied to the terms.

Considering continuity for incompressible flow ($\nabla \cdot \mathbf{V} = 0$). This results in two equations, one continuity equation for the mean values (Equation 3.10) and one for the fluctuations values (Equation 3.11)

$$\frac{\partial \overline{U}}{\partial t} + \frac{\partial \overline{V}}{\partial t} + \frac{\partial \overline{W}}{\partial t} = 0 \tag{3.10}$$

$$\frac{\partial u'}{\partial t} + \frac{\partial v'}{\partial t} + \frac{\partial w'}{\partial t} = 0 \tag{3.11}$$

Averaging the NSE gives Equation 3.12.

$$\rho \frac{D\overline{\mathbf{U}}}{Dt} + \rho \frac{\partial}{\partial x_j} \left(\overline{u_i' u_j'} \right) = \rho \mathbf{g} - \nabla \overline{p} + \mu \nabla^2 \overline{\mathbf{U}} \tag{3.12}$$

Rearranging Equation 3.12 and displaying the inertia terms as stresses[1] yields Equation 3.13.

$$\rho \frac{D\overline{\mathbf{U}}}{Dt} = \rho \mathbf{g} - \nabla \overline{p} + \mu \nabla \cdot \tau_{ij} \tag{3.13}$$

where

$$\tau_{ij} = \mu \left(\frac{\partial u_i}{\partial x_j} + \frac{\partial u_j}{\partial x_i} \right) - \rho \overline{u_i' u_j'} \tag{3.14}$$

The last term in Equation 3.14 represent the turbulent shear stress which has to be modelled. Many approaches have been put forth,

[1] strictly not true

from zero-equation models to models using multiple equations to model the term. These model makes it possible to calculate the turbulent shear and in the way close the equation system. The equations used in the models calculates different parameters in the problem, typically turbulent kinetic energy, k, and dissipation, ϵ, or a product of the two.

In the $k-\epsilon$ model the kinetic energy, $k = \overline{(u_i' u_i')}/2$, and dissipation, ϵ are calculated using transport equations.

$$\frac{\partial k}{\partial t} + U_j \frac{\partial k}{\partial x_j} = \frac{\partial}{\partial x_j}\left(\frac{\nu_t}{\sigma_k}\frac{\partial k}{\partial x_j}\right) + P_k - \epsilon \tag{3.15}$$

$$\frac{\partial \epsilon}{\partial t} + U_j \frac{\partial \epsilon}{\partial x_j} = \frac{\partial}{\partial x_j}\left(\frac{\nu_t}{\sigma_\epsilon}\frac{\partial \epsilon}{\partial x_j}\right) + \frac{\epsilon}{k}\left(C_{\epsilon 1} P_k - C_{\epsilon 2}\epsilon\right) \tag{3.16}$$

The production of k is given as

$$P_k = 2\nu_T S_{ij} \frac{\partial U_i}{\partial x_j} \tag{3.17}$$

$$S_{ij} = \frac{1}{2}\left(\frac{\partial U_i}{\partial x_j} + \frac{\partial U_j}{\partial x_i}\right) \tag{3.18}$$

The turbulent viscosity, ν_t, relating the begin effected by the kinetic energy and turbulent dissipation as

$$\nu_t = C_\mu' \frac{k^2}{\epsilon} \tag{3.19}$$

σ_k and σ_ϵ are the effective Prandtl numbers, and relate the connects the momentum eddy viscosity to the dissipation of k and ϵ, $\sigma = \nu_t/\nu_k$ and $\sigma_\epsilon = \nu_t/\nu_\epsilon$. Both σ_k and σ_ϵ, together with $C_\mu', C_{\epsilon 1}$ and $C_{\epsilon 2}$ are constants that are slightly dependent on the flow pattern. [26]

3.3.2 Modelling of turbulence in hydraulic jumps

Pothof and Clemes (2009) [34] studied how to best model the turbulence in hydraulic jump. Finding better turbulence models, gives better predictions for the pressure drop in pipes. The pressure drop is an important parameters when the flow contains gas pockets and the static head is negligible.

In a hydraulic jump, the gas entrainment is essentially a advection-diffusion problem, which the authors found to be already studied in the literature. The model needed here is however one that can be used both for fully developed boundary layer flow, and in decelerating jet flows. In order to this, the Eddy viscosity concept was used, and the focus was on finding a general Eddy viscosity model based on a priori knowledge of the energy losses in hydraulic jumps.

3.4 Summary of earlier simulations

3.4.1 Boundary conditions

Considering the set up of boundary conditions for simulation of slug, Frank [35] summarized different approaches. The first is the case of a 'frozen slug' where the slug is kept still in the computational domain with moving wall around it. The second it a set up with a periodic domain. Using a periodic domain, a driving force has to be included and the size of the geometrical domain has to designed large enough to avoid it affecting the flow. In order to set up the domain correctly for the these two cases, knowledge of slug lengths, slug periods and time scales/velocities have to be known in order to design a domain not affecting the flow. The last, and most accurate approach, is to use a long domain to simulate the flow. Although

being the most accurate approach, this approach is also the one with highest computational costs.

Frank compared the cases using periodic boundary conditions and simulating the whole pipe length, setting the final pipe length to the same. A wave function was used at to induce wave in stratified flow and transition to slug flow. For the periodic boundary condition case a pipe length of approximately 10% longer than an observed mean slug length at same condition was chosen. Although the periodic boundary conditions preformed well for the simulation, some disadvantages where emphasized. The first being the need for a priori known pressure drops and the second that the length of the periodic domain might affect the length scales and period of the simulated slug. When simulating the whole pipe the same wave function was used as an inlet condition. The outlet boundary condition was an average static pressure outlet with a relative pressure of zero. . A decrease in the liquid velocity due to the wall friction was found. This contributed to an increase of the water level in the pipe. The length of the formed slug was approximately constant until in closed on the outlet where the length increased.

Studying how a single TB moves in vertical pipes, Taha and Cui [22] set up their domain with moving boundary conditions. The wall move with the same velocity as the TB had. The wall velocity was tested and adjusted until the bubble was stationary in the domain. The domain was assumed axial symmetric.

Mo et al. [13] used a length scale model to model the boundary conditions for the turbulence on the solid walls and interfaces in their Quasi-3D simulation, see Section 3.4.4. In a length scale model, the length scales of turbulence is set as boundary conditions at both solid walls and interfaces.

3.4.2 Turbulence

Taha and Cui [22] used mass balances to check for turbulence in the film around the TB in vertical pipe. When the Reynolds number indicated that turbulence would be present, the RNG $k-\epsilon$ turbulence model was introduced. For turbulent films the last row of cells near the wall was divided into three new layers. This was done in order to ensure that the turbulence would be grid independent.

In the model of Mo et al. [13] the turbulent energy equations were solved for each phase, estimating the turbulent viscosity and dissipation rate for the different phase by equation depending on the turbulent kinetic energy.

Frank [35] tested different turbulence models for simulating the transition to slug flow using wave functions. Both homogeneous and fluid-dependent turbulence $k-\omega$ models show to produce unphysical gas velocities at the free surface and too little damping of the turbulence at the interface. To ensure better damping, additional damping was introduced into the ω equation.

3.4.3 Multiphase modelling

The observed formation of waves, droplets and liquid ligaments at the slug front which will contribute to the gas entrainment. A one-fluid model (homogeneous) will calculate the flow with the same velocity for both phases, demixing of the phases will only happen because of the 3-D motion. Therefore using VOF will possibly lead to a 'generally different behaviour of the multiphase mixture in areas with higher gas entrainment, and to a higher demixing time.' [35]

An Euler-Euler approach will regard both phases as a continua, and is based on mass-weighted averaged mass and momentum transport equations for both phases. The phases are then coupled using an

equation for the interfacial drag. Frank used this approach and combined it with a free-surface model, and thereby neglecting the surface tension between the phases.

Taha and Cui [22] used a one-fluid approach with volume of fluid to model the motion of a single Taylor bubble in vertical pipes.

3.4.4 Geometric dimensions

The importance of using three dimensions instead of two when simulating slug flow was stressed by Frank [35]. This was done based on the importance of the wall friction and blockage of the pipe cross-section for transition from stratified flow to slug flow. A 2D simulation will neglect the side-wall effects on the flow, which may have significant influence on the slug formation.

Taha and Cui [22] assumed axissymmetric flow in the vertical pipe, so the domain was only set up from the center of the pipe to the wall in a plane. At the pipe center line axis-symmetric boundary condition was applied.

Quasi 3D-modelling Mo et al. [13] presented some progress done with Quasi-3D simulations. The need for progress in 3D simulations arise due to the large impact the wall friction will have on the slug flow, and that a total blockage of the domain is easily done in a 2D channel but not as easy in a 3D pipe. The model presented by Mo et al. is set up for three phases and a phase is considered continuous is the local void fraction is above 0.5. The three phases make up nine different fields, considering the dispersion of two phases in the third. The Quasi 3D is set up by slicing the pipe in longitudinal direction. The model equations in 3D are then averaged over the different slices and positions in the pipe. The approach showed to be able to reproduce Taylor bubble velocity well for different inclinations, especially for vertical pipes, the onset of slugging, and the slug frequency. Using

a Quasi 3D approach reduces the computer power and time needed significantly since the numerics are solved for two dimensions.

3.4.5 Flow regime transition

Issa and Kempf [36] presented in 2003 a mechanistic model, based on the numerical solution of one-dimensional transient two-fluid model equations to predict hydrodynamic slug initiation, growth and subsequent development into continuous slug flow in pipelines'. Modelling a transient model, reduces the need for equations to solve flow transitions, slug formation and slug dynamics.

The study considered how to solve numerically flow instabilities and found it necessary to have a high grid density in order to let the instabilities grow. Otherwise, the instabilities would be suppressed by the numerical diffusion and therefore not give the instabilities the possibility to eventually induce a flow regime transition.

Friction factors

Using the two-fluid model a closure relationship between the governing equations for the phases are needed. These closures can be calculated evaluating the friction factors, f_{gw}, f_{lw} and f_i, the indices meaning gas-wall, liquid-wall and interfacial. Considering different friction factor models, the transition to slug flow was found to be most effected by the friction factor model used for f_{lw}, but hardly effected by the models choosen for f_{gw} and f_i. The authors summarized the best frictions factors as can be seen in Tabel 3.1.

[36]

Table 3.1: Friction factors for laminar flow

f_g	$\frac{16}{Re_g}$	Hagen-Poiseulle formula
f_i	$\frac{16}{Re_i}$	Hagen-Poiseulle formula
f_l	$\frac{24}{Re_l}$	Hand(1991)/ Spedding and Hand(1997)

Table 3.2: Friction factors for turbulent flow

f_g	$0.046\,(Re_g)^{-0.2}$	Taitel and Dukler(1976)
f_i	$0.046\,(Re_i)^{-0.2}$	Taitel and Dukler(1976)
f_l	$0.0262\,(\alpha_l\ Re_l)^{-0.139}$	Hand(1991)/ Spedding and Hand(1997)

With the Reynolds numbers given as follows:

$$Re_g = \frac{4A_g u_g \rho_g}{(S_g + S_i)\,\mu_g} \tag{3.20}$$

$$Re_i = \frac{4A_g |u_g - u_l| \rho_g}{(S_g + S_i)\mu_g} \tag{3.21}$$

$$Re_l = \frac{D\ U_{sl} \rho_l}{\mu_l} \tag{3.22}$$

Bonizzi and Issa, 2003 [37], used the same mechanistic approach as Issa and Kempf, 2003 [36] for simulation of gas entrainment in horizontal slug flow. The model was adjusted to include a scalar function for the calculation of gas bubbles into the liquid phase, and the gas entrainment rate is in the form of a closure relation. The friction factor for the liquid phase was adjusted to represent an effective friction factor, f_d. For the calculations of the aerated liquid slug, a new phase in introduced being the liquid phase together with dispersed entrained gas bubbles, phase M. Thus,

$$\alpha_G + \alpha_M = 1 \tag{3.23}$$

where $\alpha_M = \alpha_L + \alpha_B$. The subscripts G, L and B represent the gas bubble, the liquid phase and the dispersed bubbles, respectively. The mixture density is given as

$$\rho_M = \rho_L (1 - \alpha_B) + \rho_G \alpha_B \tag{3.24}$$

The liquid-wall friction factor an effective friction factor, f_d taking into consideration the change of friction factor for an aerated liquid body is used.

$$f_d = \phi_d f_L \tag{3.25}$$

$$\phi_d = \frac{1}{1 - \alpha_B} \left[1 + 15.3 \frac{\alpha_B}{\sqrt{(1 - \alpha_B)}} \frac{u_\infty}{u_M} \right] \tag{3.26}$$

ϕ_d will be unity when parts not included in the aerated liquid slug is considered. f_L is the friction factor as used by Issa and Kempf.

3.5 Simulation of gas entrainment at propagating slug front

The set-up presented in this section is the same presented by Hua, Nordbø and Foss [38] in 'CFD modelling of gas entrainment at a propagating slug front' *presented in Trondheim at the 10th International Conference on CFD in Oil & Gas, Metallurgical and Process Industries, 17-19 June, 2014*

Simulation domain and parameters

The simulation domain was set-up to focus on the gas entrainment from the TB tail and the domain therefore covered the TB tail and the liquid slug, see Figure 3.1.

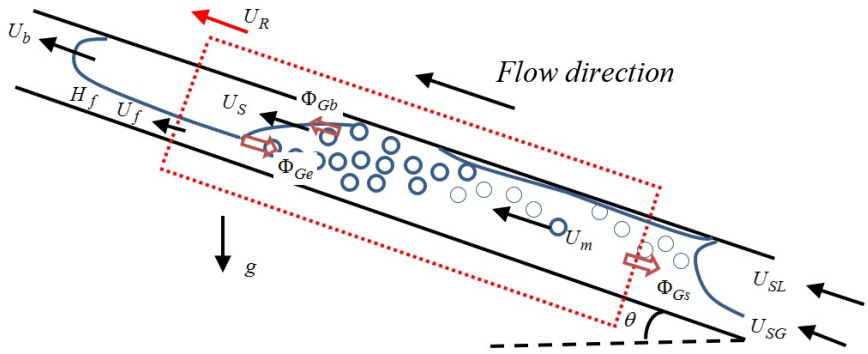

Figure 3.1: Simulation domain containing slug front

To easier study the gas entrainment at the slug front, a moving reference frame was applied. The reference frame was given the same velocity as the TB. The set-up is shown schematically in Figure 3.2.

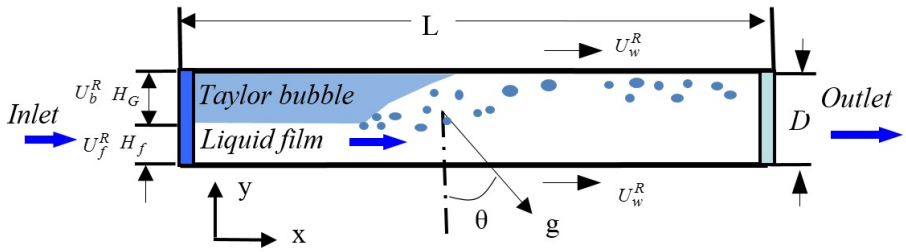

Figure 3.2: Simulation domain

Using a moving reference frame simplifies the study of the entrainment processes at the slug front, keeping this at the position when first stabilized. The the speed of the moving wall will therefore represent the speed of the TB in a normal slug, ($U_W^R = U_b$). The diameter of the pipe was set to $D = 0.1\ m$, and the length $L = 20D$. The fluid properties for the different phases were set to represent a water-air system. The grid space was set to 1 mm, giving 100 cells for each diameter. At the pipe walls no-slip boundary conditions were applied. The inlet condition of the liquid film was a relative inlet velocity of ($U_f^R = U_b - U_f$), and a liquid film height of H_f. The gas inlet velocity in the TB was set to $U_G^R = 0$, since the walls are moving with the TB velocity. The pipe inclination was adjusted by changing the gravity vectors in the pipe coordinate system. The time step was set to $1.0 \cdot \times 10^{-4}\ s$, and a second order temporal discretization scheme was applied. The gravitational vectors were adjusted in order to simulate inclined pipes with the inclination of θ.

Mathematical formulations

For the simulation a one-fluid approach was used. The gas-liquid interface is tracked using the VOF method explained in Section 3.2.2.

The density in the momentum equation may therefore not be eliminated as already done in Equation 3.1 since this is no longer constant

despite fluids that are assumed incompressible. Including varying density and dynamic viscosity as in Equations 3.27 and 3.28.

$$\rho = \rho_l (1 - \alpha) + \rho_g \cdot \alpha \tag{3.27}$$

$$\mu = \mu_l (1 - \alpha) + \mu_g \cdot \alpha \tag{3.28}$$

Introducing the VOF calculations, and the varying density and viscosity in the momentum equation, and removing the contribution from the hydrostatic pressure, the momentum equation can be expressed as

$$\frac{\partial \rho \mathbf{u}}{\partial t} + \nabla \cdot (\rho \mathbf{u}\mathbf{u}) = -\nabla p + \nabla \cdot (\mu_e \nabla \mathbf{u}) + \mathbf{f}_{ST} + (\rho - \rho_L)\,\mathbf{g} \tag{3.29}$$

$\mathbf{f}_{ST}$ is given in Equation 3.7, and $\mu_e = \mu + \mu_t$ combining the fluid viscosity with the turbulent viscosity calculated with the $k-\epsilon$ method presented in Section 3.3.1.

3.6 Simulation results

The results in this section are the same as presented by Hua, Nordbø and Foss in 'CFD modelling of Gas Entrainment at Propagating Slug Front' *at the 10th International Conference on CFD in Oil & Gas, Metallurgical and Process industries, June 2013, Norway* [38].

The studied parameters were the pressure drop, the turbulent kinetic energy (TKE), the gas entrainment rate Φ_G, the void fraction in the wake zone α_w and the void fraction in the slug body α_s.

Pro and cons with simulation: Possible to vary only one parameter at the time, indicating the parameters having greater effect than others at the gas entrainment.

3.6.1 Base case

A base case simulation was set up using the values listed in Table 3.3. This base case is used in the following Section 3.6.1 and 3.6.1 to explain the gas entrainment in the slug flow and how the domain was divided into different parts in order to study the .

Table 3.3: Initial parameters for base case simulation

Bubble propagation velocity	U_w^R	1.5 m/s
Film velocity	U_f^R	1.0 m/s
Film height	H_f	0.4
Pipe inclination	θ	10°

Gas entrainment measurement

The simulation domain moving with the slug front makes it possible to track the size of the Taylor bubble in the domain in addition to the amount of gas leaving the slug body. Doing this over time to both see how the volume of the bubble changes with time due to the dynamic behaviour at the slug front as well as the time-averaged flux of gas into the slug body. The dynamic behaviour at the slug front arises due to the different entrainment mechanism, entrainment of small bubble at base of jump, entrainment of larger bubbles due to impingement and back-flow and coalescence of entrained bubbles with the Taylor bubble. Figures 3.3 and 3.4 show parallel snapshots from the simulation showing how gas bubbles are entrained in the liquid slug. Figure 3.3 display the void fraction in the slug body, and Figure 3.4 is presented with the local velocity vectors in order to more easily study the vortices in the slug body. The snapshots were taken with an interval of 0.08 s, and for a total time of 0.40 s. Red color represent gas with a calculated void fraction in the cell higher than 0.2. Blue color is liquid with a void fraction of 0 in the cell. The yellow arrows in the figures highlights the entrainment of larger bubbles due to the impingement of a liquid jet initiated from the interaction between the liquid film with the liquid slug body and the vortex just behind the slug front, see Figure 3.3a. In Figure 3.3b it can be seen how the liquid jet moves into the TB, and in Figure 3.3c how a larger bubble is fragmented from the TB by the liquid jet. This bubble is transported into the slug body, Figure 3.3d, and when it comes in contact with the vortices in the liquid it is move to the lower part of the pipe and fragmented further as seen in Figures 3.4e and 3.4f.

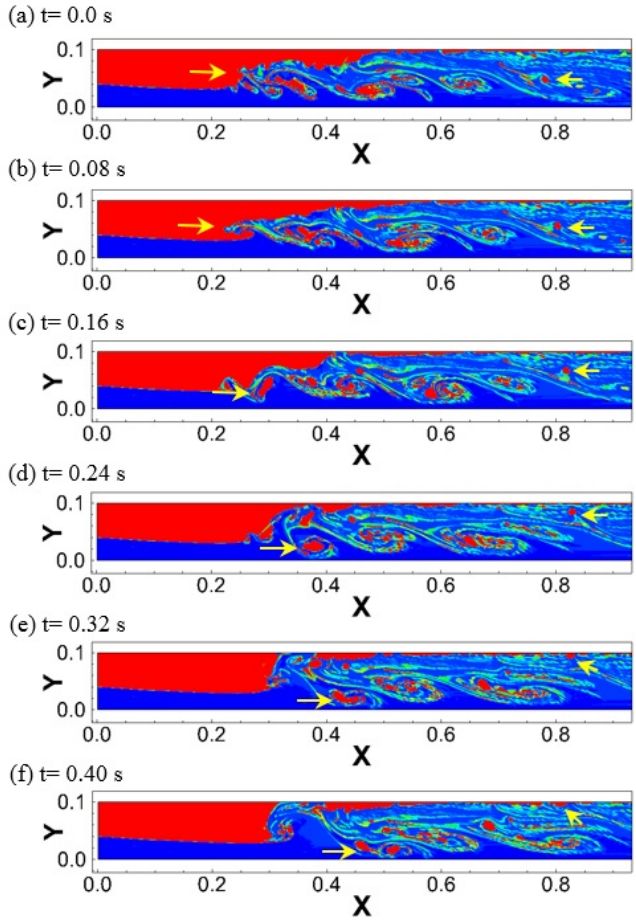

Figure 3.3: Snapshots of gas entrainment at different times

In the developed slug body both figures show a yellow arrow highlighting how a larger bubble rises in the pipe and end up at the top wall of the pipe. As seen in Figure 3.4 the turbulence intensity decrease, seen as decreased size of velocity vectors, allowing the bubble to rise due to buoyancy. A thin gas layer is formed at the top of the pipe, called the Taylor bubble tail. Due to the circulation of the vortices, this layer will slowly move back towards the TB and recoalesce

with this.

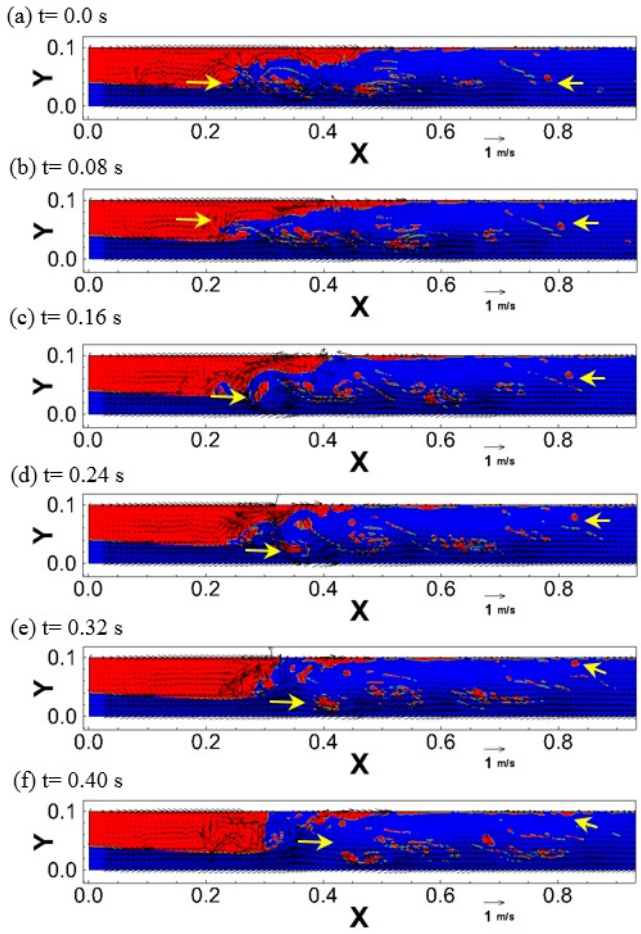

Figure 3.4: Snapshots of gas entrainment at different times with velocity vectors

As seen in Figures 3.3 and 3.4, the gas entrainment in the simulation is dependent both an entrainment into the slug, as well as a backflow of larger bubbles recoalesing with the TB. For the base case, the volume changes of both the total gas volume in the domain, $\dot{V}_G$, and

the change of the TB size, $\dot{V}_b$, is shown in Figure 3.5.

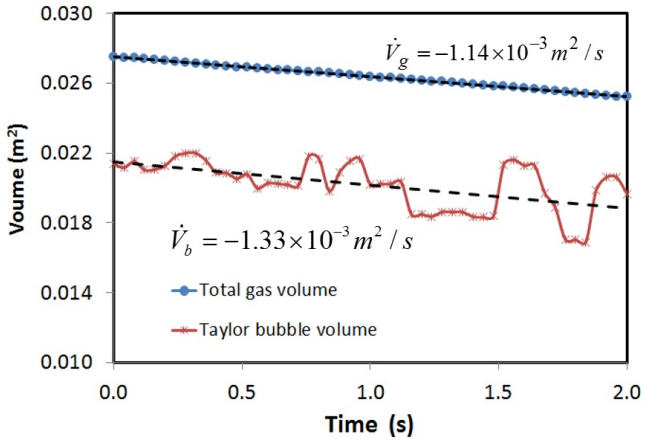

Figure 3.5: Total gas volume change and Taylor bubble volume change for base case scenario

The gas shedding rate out of the domain was normalized to a velocity rate using the diameter, $\Phi_{Gs} = -\dot{V}_G/D$. The entrainment velocity is equally normalized as an entrainment velocity, $\Phi_{Ge} = -\dot{V}_b/D$. An average of these two velocities, $\Phi_G = (\Phi_{Ge} + \Phi_{Gs})/2$, was used in this study to quantify the gas entrainment in the slug.

For other values than the gas entrainment rate, the domain was average for a time periode of about 2 seconds. Figure 3.6 show in (a) an the average void fraction in the slug, and in (b) an averaged velocity field. The average void fraction in Figure 3.6a shows how the void fraction vary clearly between the wake zone, with an average of high void fraction, and the developed slug body with lower average void fraction. The velocity vectors in Figure 3.6b show that the gas at the interface between the liquid slug front and the TB flows back towards the main TB body.

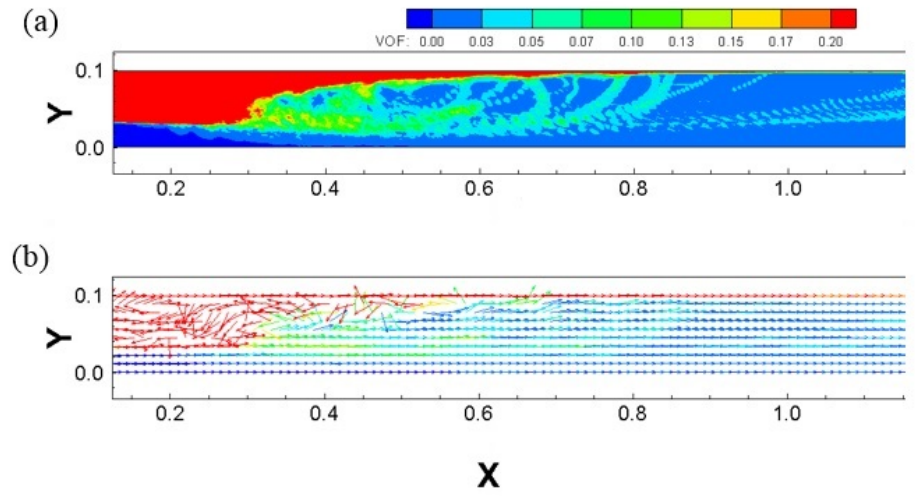

Figure 3.6: Time averaged values for (a) void fraction and (b) fluid flow direction

Sectioning of the domain

Due to the different mechanisms occurring at the slug front being responsible for the gas entrainment and mechanism resulting in back-flow and recoalescence of entrained bubbles with the Taylor bubble, a sectioning strategy of the simulation domain was used to enable studies of the different parts of the slug. The recirculation will be highest at the slug front(B), and lowest in the Taylor bubble region(A) and the developed slug(D) body. There will also be recirculation in the wake zone (C), but not as strong as at the slug front. A typical section of the domain is shown in Figure 3.7.

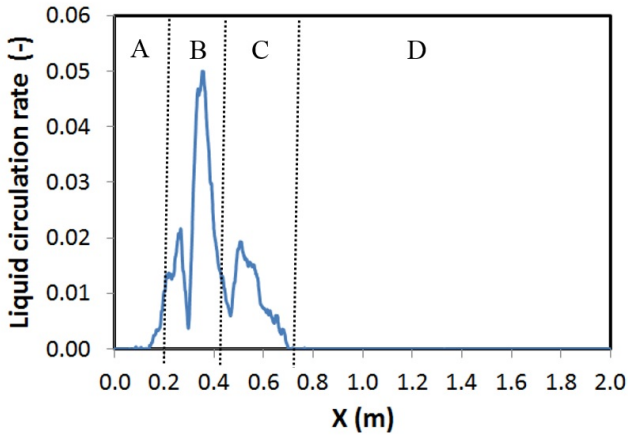

Figure 3.7: Variation of liquid recirculation rate along pipe axis with corresponding regions

Figure 3.8 shows the variations of the TKE withing the different sections. The TKE will increase in the liquid film and reach it's highest value at the slug front. In the wake zone the TKE reaches to a medium high, steady value before decaying in the developed slug body.

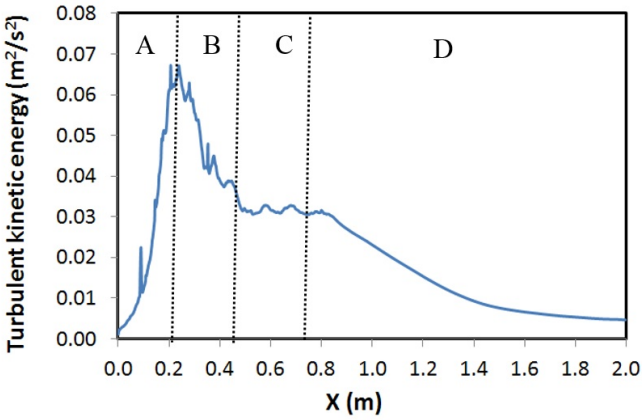

Figure 3.8: Variation of turbulent kinetic energy along pipe axis with corresponding regions

The pressure drop in the slug flow is shown in Figure 3.9. The hydrostatic pressure has been removed from the static pressure calculated in the simulation.In the TB zone a low pressure region is formed, since the TB is travelling faster than the liquid slug body. This induces an acceleration of the slug front, which leads to the formation of a liquid jet. The liquid slug body jet will interact with the liquid film, which leads to one of the main mechanisms for gas entrainment of the slug front.

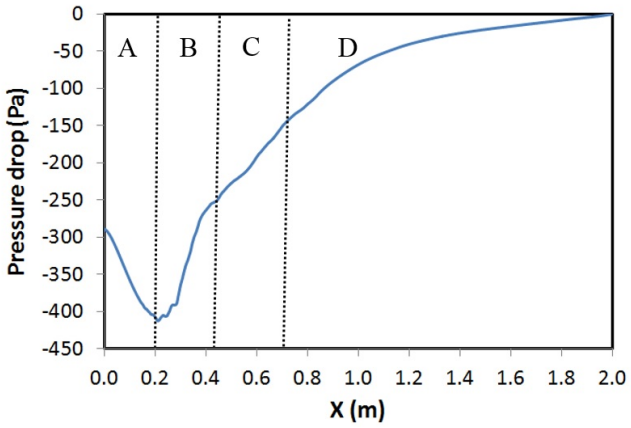

Figure 3.9: Pressure drop along pipe axis with corresponding regions

3.6.2 Effect of different parameters

Taylor Bubble propagation velocity

The effect of the TB propagation velocity was studied evaluating five different cases with different velocity of the moving reference frame, U_w^R. As shown in Figure 3.10 the overall pressure drop increased with increasing bubble propagation velocity. A slightly slower regeneration of the pressure in the slug body was observed. The turbulent kinetic energy at the front was found to be highest for a propagation velocity of 1.5 m/s. The wake zone was found to have highest values for the lowest propagation velocities, and lowest for the case with $U_b = 1.5m/s$, see Figure 3.11.

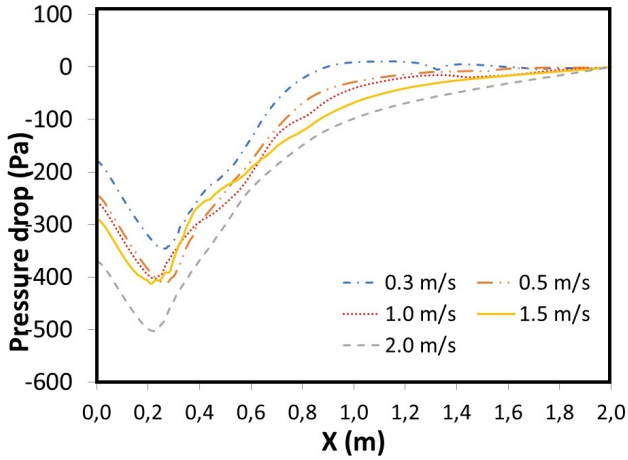

Figure 3.10: Pressure drop for cases with different bubble propagation velocity

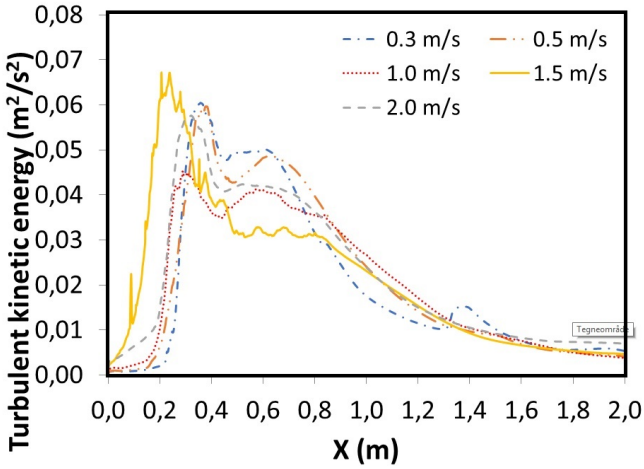

Figure 3.11: Turbulent kinetic energy for cases with different bubble propagation velocity

The gas entrainment rate, Φ_G, was found to increase with increasing bubble propagation velocity. Figure 3.12 show how the relative volume of the TB changed with time during the simulation. The TB volumes for a sequence of 2 s were calculated and divided by the TB volume at the end of the sequence make the numbers comparable for different TB volumes. The fluctuations of the lines in the figure are indications of entrainment and backflow of larger bubbles from and back into the TB, respectively. As can be seen in the figure, the fluctuations increase with increasing bubble propagation velocity, implying that entrainment of larger bubbles play a more significant role in the gas entrainment. The general decaying trend indicate the entrainment of small droplets without significant effect on the TB volume for one time step to the next. The case with $U_b = 1.5$ m/s has the largest fluctuations and this corresponds to that this has the highest slug front turbulent kinetic energy as show in Figure 3.11.

Table 3.4: Effect of bubble travelling velocity U_b on gas entrainment, ϕ_G, and void fractions in wake zone , α_w, and in developed slug zone, α_s

$U_b(m/s)$	0.3	0.5	1.0	1.5	2.0
$\phi_G(m/s)$	2.84E-3	2. 88E-3	8.46E-3	1.24E-2	1.35E-2
α_w	3.88E-2	1.88E-1	1.66E-1	1.12E-1	2.16E-1
α_s	3.10E-2	2.35E-2	3.44E-2	2.57E-2	2.71E-2

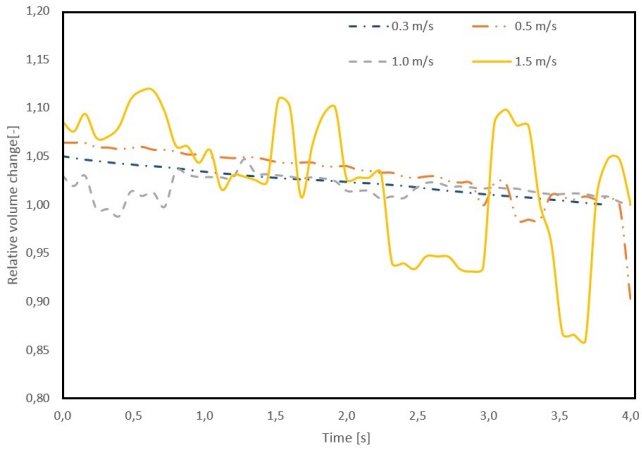

Figure 3.12: Relative change of Taylor bubble with time for cases with different bubble propagation velocity

Film velocity

Increasing the inlet liquid film velocity, the was found to increase the pressure drop for the liquid film, see Figure 3.13. The pressure drop for a liquid film is dependent on the friction between the wall and the liquid, which will increase with increasing liquid velocity. At the same time, increased liquid film velocity will increase the shearing between the liquid in the slug and the liquid film. This gave an increase in the turbulent kinetic energy in the slug, as shown in Figure 3.14. The increased momentum was also found to slightly shift the front upstream, which is due to the increase intensity of the resulting hydraulic jump.

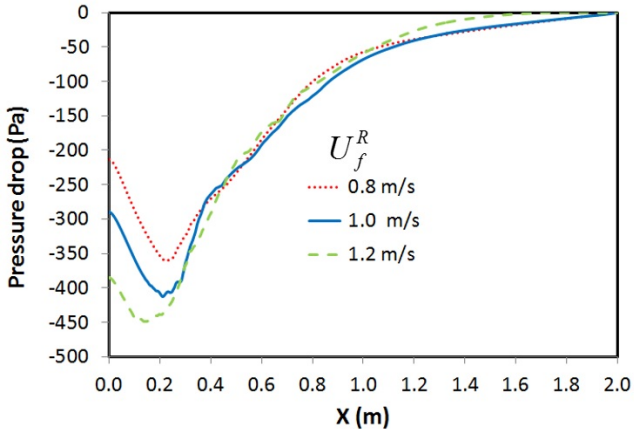

Figure 3.13: Pressure drop for cases with different liquid film velocity

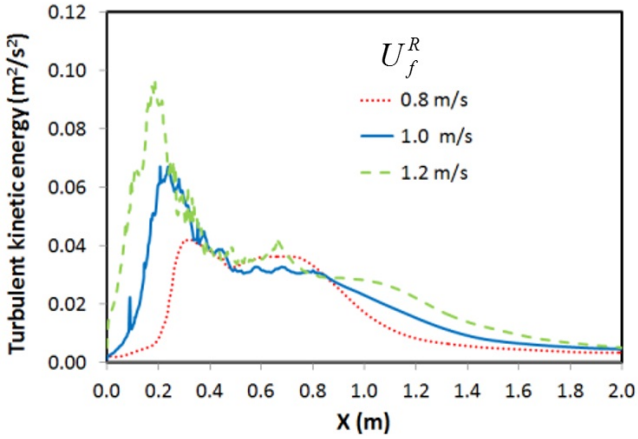

Figure 3.14: Turbulent kinetic energy for cases with different liquid film velocity

The increase of liquid film velocity was found to have an positive effect an the gas entrainment, see Table 3.5

Table 3.5: Effect of liquid film velocity U_f on gas entrainment, ϕ_G, and void fractions in wake zone , α_w, and in developed slug zone, α_s

$U_f^R(m/s)$	0.8	1.0	1.2
$\phi_G(m/s)$	6.11E-3	1.24E-2	1.27E-2
α_w	1.74E-1	1.12E-1	2.18E-1
α_s	2.10E-2	2.57E-2	3.28E-2

The relative volume change of the TB is shown in Figure 3.15. The volume changes strongly with time for a film velocity of 1.2 m/s, indicating that this velocity increases the turbulent kinetic energy in the slug enough to generate liquid jets on a frequent basis.

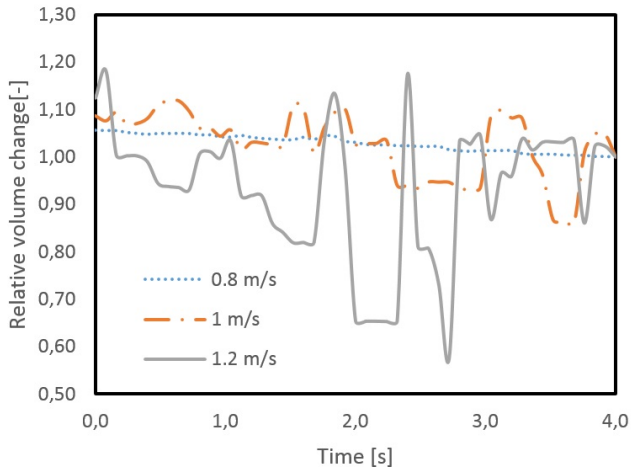

Figure 3.15: Relative change of Taylor bubble with time for cases with different liquid film velocity velocity

Film height

When varying the initial film height in the TB zone, the pressure drop was found to vary little for low film height (0.2 and 0.3). The pressure

drop increased significantly for a film height of 0.4, but decrease when the film height was increased further. With a low film hight, the liquid film has little momentum to transfer to the liquid slug resulting in a low values for the turbulent kinetic energy. The opposite situations is the case for a high liquid film, since in this case the slug front has little momentum, resulting in low values for the turbulent kinetic energy. At an intermediate value of film height, a significantly higher value for the turbulent kinetic energy was found. At intermediate film height values, both the liquid film and the liquid slug will contribute to generation of turbulent kinetic energy.

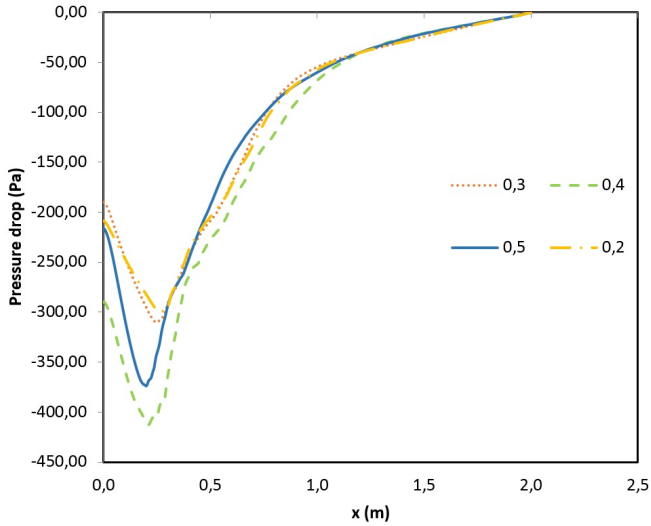

Figure 3.16: Pressure drop for cases with different liquid film height

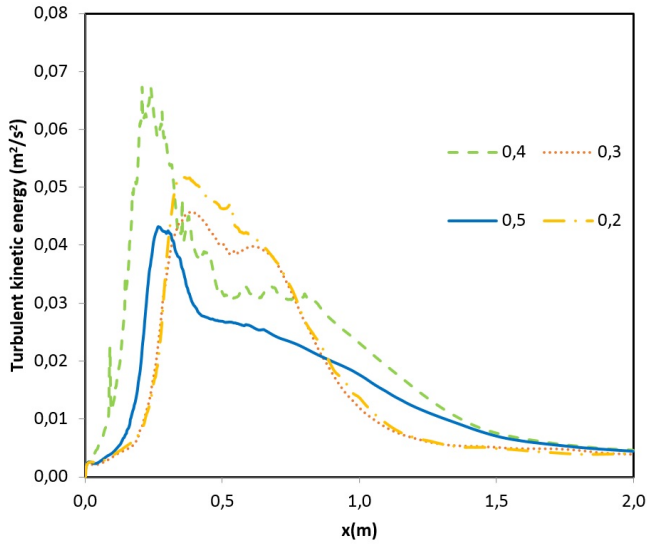

Figure 3.17: Turbulent kinetic energy for cases with different liquid film height

The gas entrainment was found to increase with increasing liquid film hight, see Table 3.6.

Table 3.6: Effect of liquid film height H_f on gas entrainment, ϕ_G, and void fractions in wake zone , α_w, and in developed slug zone, α_s

$H_f(m/s)$	0.2	0.3	0.4	0.5
$\phi_G(m/s)$	3.00E-3	5.03E-3	1.24E-2	1.12E-2
α_w	4.97E-2	2.00E-1	1.12E-1	1.89E-1
α_s	2.72E-2	2.23E-2	2.57E-2	2.31E-2

Figure 3.18 shows the relative change of the TB volume as a function of time. The only case showing large fluctuations of the TB volume, is for $H_f = 0.4$. As shown in Figure 3.17 this is also the case with the highest values for the turbulent kinetic energy at the front, and

in Figure 3.16 the strongest pressure drop at the front. These factors may give rise the a slug front with high intensity and there producing frequent liquid jets.

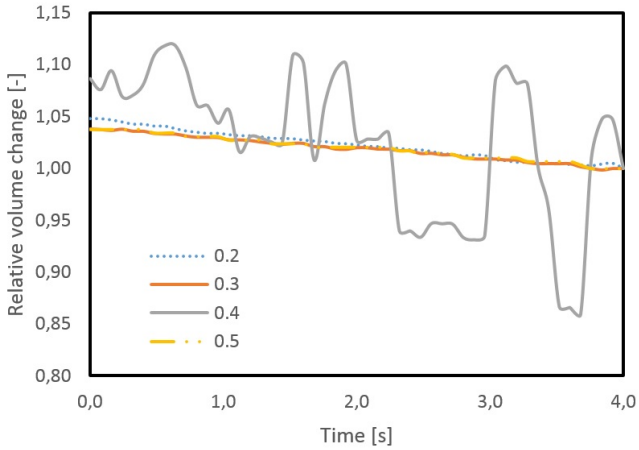

Figure 3.18: Relative change of Taylor bubble with time for cases with different liquid film height

Pipe inclination

When changing the pipe inclination the pressure drop at the liquid slug front was found to increase significantly, despite the unaffected total pressure drop, see Figure 3.19. The turbulent kinetic energy was also found to increase with increasing pipe inclination, see Figure 3.20.

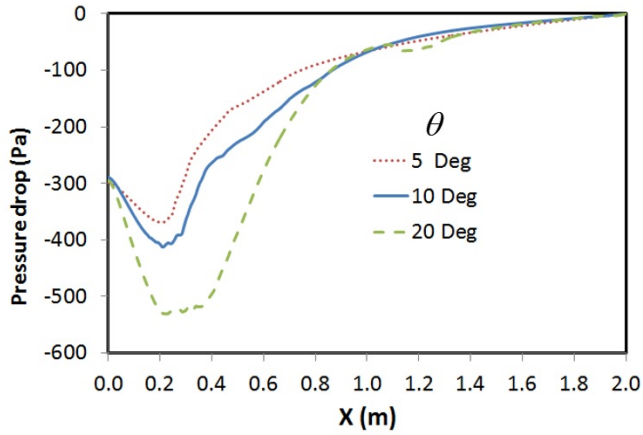

Figure 3.19: Pressure drop for cases with different pipe inclination

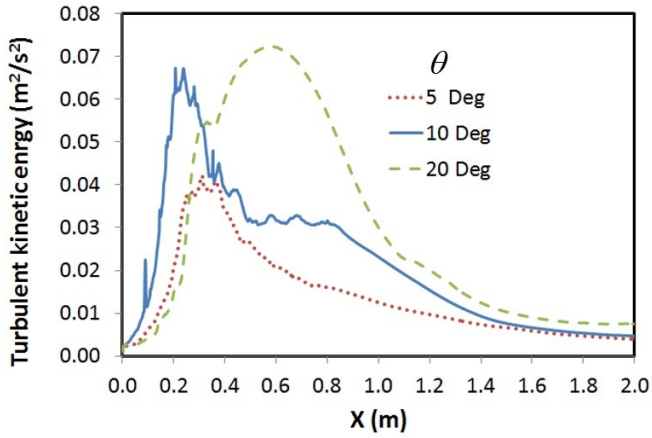

Figure 3.20: Turbulent kinetic energy for cases with different pipe inclination

As can be seen in Table 3.7, the gas entrainment rate increased for increasing pipe inclination. Figure 3.18 shows the relative change of the TB volume as a function of the. The variation is strongest for

$\theta = 10°$ and lowest for $\theta = 20°$. Comparing this figure to Figure 3.17 it is evident that the turbulent kinetic energy for $\theta = 10°$ is mainly at the slug front giving rise to liquid jets, while for $\theta = 20°$ the turbulent kinetic energy is more distributed into the slug body. The gravity will work in the opposite direction of the liquid jet for a inclined pie, which also may explain the lowered large bubble fragmentation.

Table 3.7: Effect of pipe inclination,θ on gas entrainment, ϕ_G, and void fractions in wake zone , α_w, and in developed slug zone, α_s

θ	5°	10°	20°
$\phi_G(m/s)$	7.50E-3	1.24E-3	1.28E-2
α_w	1.40E-1	1.12E-1	9.59E-2
α_s	2.09E-2	2.57E-2	3.79E-2

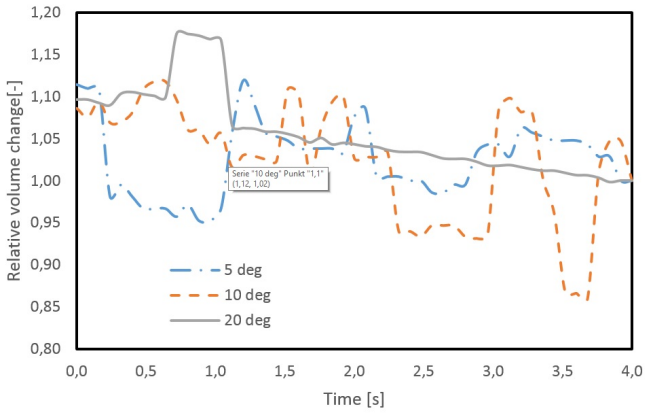

Figure 3.21: Relative change of Taylor bubble with time for cases with different pipe inclination

3.7 Summary and discussion

By using a simulation of the gas entrainment in slug flow, it has been possible study the effect different parameters have on the entrainment. The results show that the gas entrainment at the slug front will be dependent on the shear between the slug front and the liquid film. The recirculation in the slug body will contribute to different void fractions in the wake zone and the developed slug body. The turbulent kinetic energy in the flow was used to study the interaction between the film and the slug body. Changing different parameters, reveal that multiple parameters are affecting the interaction, and that quantifying the momentum transfer between the liquid film and the liquid slug body with the turbulence kinetic energy can be used as a way to study the gas entrainment and void fraction in a slug. Monitoring the volume of the TB reveal a tendency of liquid jets fragmenting and entraining larger bubbles from the TB tail that corresponded to cases with high turbulent kinetic energy at the front. The liquid film height was found to have largest momentum exchange at intermediate heights. Too high or too low liquid film height would lower the exchange, due to lowered intensity of either the liquid film or the slug front hydraulic jump. Larger pipe inclination leads to higher pressure drop at front, and thus a higher acceleration of the slug. A bubble propagation velocity increase results in a decrease in of the pressure in the Taylor bubble. Which further leads to a larger pressure drop at the slug front. The film velocity was found to increase the turbulent kinetic energy in the slug, and lower the pressure in both the Taylor bubble and at the slug front.

The simulations did not cover physical factors, i.e. surface tension, densities and viscosities which may also influence the gas entrainment.

Part 4

Mechanistic model and experimental considerations of slug flow

Having studied the effect different parameters have on the gas entrainment in slug flows, this new knowledge was tried applied to evaluate prediction models. In order to model slug flow, a mechanistic model evaluating the different velocities and frictions the different phases are experiencing. This section serves first to present a general mechanistic balance for a unit cell slug. The mechanistic balance is applied to experimental values, making it possible to study the different factors at the slug front.

4.1 General mechanistic balance

For stationary slug, where the fractions of the different zones are constant and the unit cell concept can be used, continuity set restrictions on the different velocities and holdups.

The liquid and gas conservation equations are listed below, see Equations 4.1 and 4.2.

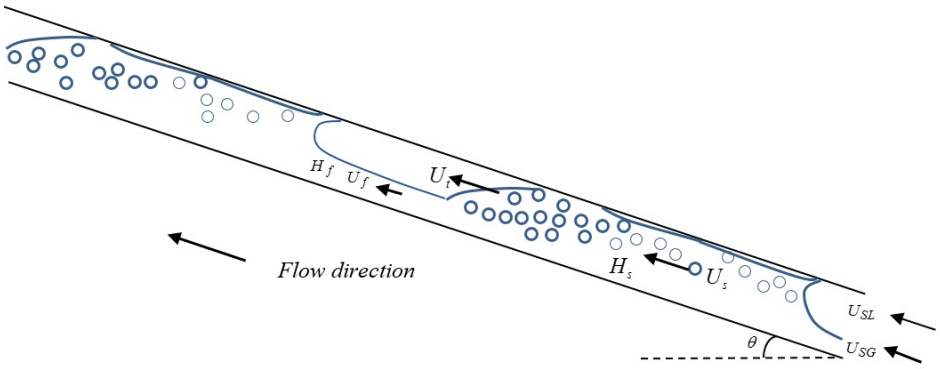

Figure 4.1: Mechanistic balance velocities

$$U_{SL} = U_s H_s \frac{l_S}{l} + U_f H_f \frac{l_f}{l} \tag{4.1}$$

$$U_{SG} = U_s \left(1 - H_s\right) \frac{l_S}{l} + U_f \left(1 - H_f\right) \frac{l_f}{l} \tag{4.2}$$

The mean velocity of the slug body is assumed to be the same as the mixture velocity of the system, see Equation 4.3.

$$U_s = U_m = U_{SL} + U_{SG} \tag{4.3}$$

Evaluating a unit slug cell travelling with a translational velocity, U_t, a balance of the liquid phase in the unit cell can be evaluated in the moving coordinate system.

$$\left(U_t - U_f\right) H_f = \left(U_t - U_s\right) H_s \tag{4.4}$$

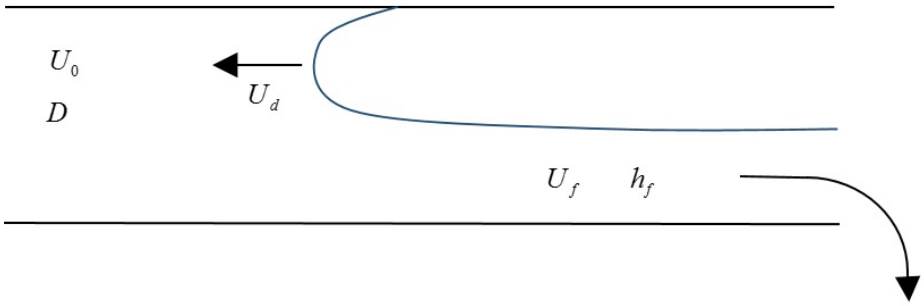

Figure 4.2: Drift velocity experiment for a bubble in stationary liquid

A common equation to calculate the translation velocity is the one presented by Nicklin in 1966, see Equation 4.5.

$$U_t = CU_m + U_d \tag{4.5}$$

U_d is the bubble drift velocity as given in Equation 4.6, and C is a constant. The drift velocity is the velocity the TB would have when the liquid flow is zero.

$$U_d = 0.54\sqrt{gD} \cdot cos(\phi) + 0.35\sqrt{gD} \cdot sin(\phi) \tag{4.6}$$

$$C = \begin{cases} 1.2 & \text{for turbulent flow} \\ 1 & \text{for laminar flow} \end{cases} \tag{4.7}$$

In addition to the mass conservation and continuity equations, the flow will be affected by the momentum of the different phases. The phases will have a pressure loss as they travel through the pipe. This pressure drop will be a result of the wall friction and the interfacial shear stresses since the flow is a two-phase flow. The liquid momentum balance for liquid film in the film zone can be seen in Equation 4.8 and the gas momentum balance in Equation 4.9.

$$-A_f \frac{dP}{dx} = \tau_f S_f - \tau_i S_i \tag{4.8}$$

$$-A_G \frac{dP}{dx} = \tau_G S_G + \tau_i S_i \tag{4.9}$$

The pressure drop for the interface, $\frac{dP}{dx}$, has to be equal for both phases, so eliminating the pressure drop for the momentum equations results in Equation 4.10.

$$\frac{\tau_f S_f - \tau_i S_i}{A_f} = \frac{\tau_G S_G + \tau_i S_i}{A_G} \tag{4.10}$$

The shear stresses in Equations 4.8 - 4.10 are defined as follows.

$$\tau_f = \frac{1}{2} f_f \rho_L |U_f| U_f \tag{4.11}$$

$$\tau_G = \frac{1}{2} f_G \rho_G |U_G| U_G \tag{4.12}$$

$$\tau_i = \frac{1}{2} f_i \rho_L |U_G - U_f| \left(U_G - U_f\right) \tag{4.13}$$

The Fanning friction factors [8] are defined as in Equation 4.14 for the liquid film, f, and as seen in Equation 4.15 for the gas in the TB.

$$f_f = \frac{C}{\left(\rho_L U_f D_{hf} / \mu_L\right)^m} \tag{4.14}$$

$$f_g = \frac{C}{\left(\rho_G U_g D_{hg} / \mu_G\right)^m} \tag{4.15}$$

The interfacial friction factor is set to a constant value, $f_i = 0.0142$.

The different geometric parameters are given in the following equation. All of which are dependent on the angle, θ, defined as in Figure 4.3. θ will be zero for a non-existing film height, and increase with increasing film heights.

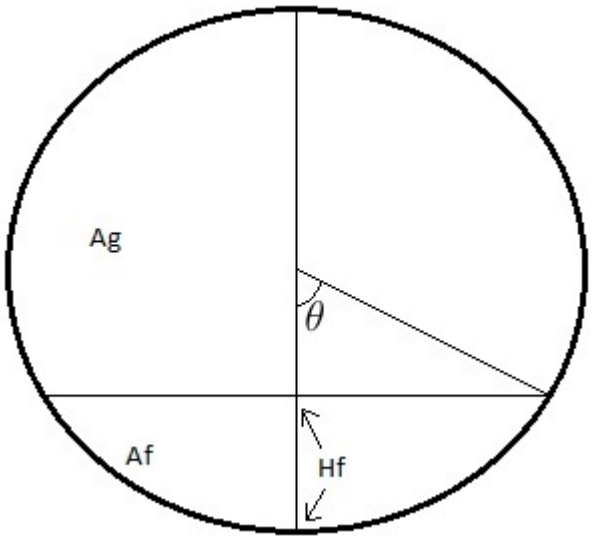

Figure 4.3: Geometric parameters in mechanistic model

With a given θ it is possible to calculate all the other geometrical parameters needed for the mechanistic model using the equations below.

$$H_f = \frac{\theta - 0.5\sin(2\theta)}{\pi} \tag{4.16}$$

$$A_f = \frac{D^2}{4}\left(\theta - 0.5\sin(2\theta)\right) \tag{4.17}$$

$$A_g = \frac{D^2}{4}\left(\pi - \theta + 0.5\sin(2\theta)\right) \tag{4.18}$$

$$S_f = D\theta, \quad S_g = D\left(\pi - \theta\right), \quad S_i = D\sin\theta \tag{4.19}$$

$$D_{hf} = \frac{4A_f}{S_f}, \quad D_{hg} = \frac{4A_g}{S_g + S_i} \tag{4.20}$$

4.1.1 Taylor Bubble Wake Model

Brauner and Ullmann presented in 2004 [39] a mechanistic model evaluating the different effects affecting the Taylor bubble (TB) wake. The Taylor Bubble Wake Model introduced take into account that the void fraction in the slug develops form the slug front, through the TB wake, to the developed liquid slug zone. Two different entrainment rates are used to calculate the gas entrainment; the gas entrainment from the tail of the TB, and the re-coalescence of entrained bubbles with the TB. The net entrainment rate is then calculated as the difference between these two, giving the overall gas entrainment rate: $\Phi_{GS} = \Phi_{Ge} - \Phi_{Gb}$.

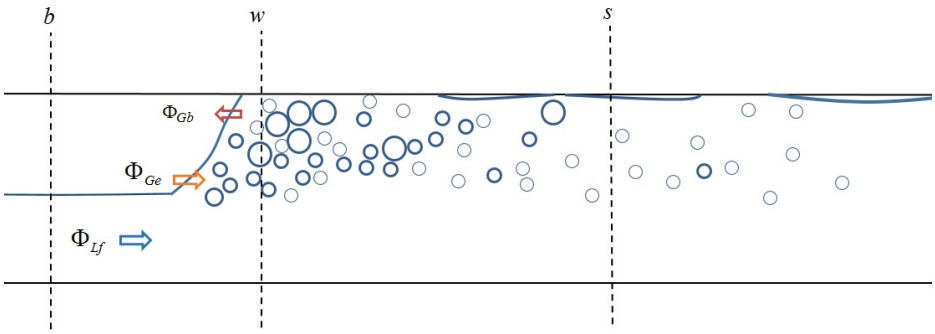

Figure 4.4: Different cross-sections for TBW

Φ_{Ge} is evaluated based on the surface energy. The flux of surface

energy is assumed proportional to the flux of turbulent energy in the liquid film penetrating the liquid slug provides.

$$\frac{1}{2}\rho_L\left(u'^2+v'^2+w'2\right)\Phi_{Lf}=C_J\frac{6\sigma}{d_{max}}\Phi_{Ge} \tag{4.21}$$

where Φ_{lf} is the flux of the liquid film

$$\Phi_{Lf}=\left(U_{GTB}-U^w_{Lf}\right)(1-\epsilon^w_{TB}) \tag{4.22}$$

The turbulence is estimated from the wall jet the liquid film makes, and the shear layer produced inside the liquid slug.

$$\left(u'^2+v'^2+w'2\right)\simeq 0.03\left(U^w_{LLS}-U^w_{Lf}\right)^2 \tag{4.23}$$

where U^w_{LLS} is the velocity of the liquid bulk and U^w_{Lf} is the velocity of the liquid film.

The backflow and re-coalescence of the entrained gas from the liquid slug to the Taylor bubble, Φ_{Gb} is set to be a function of the Taylor bubble velocity, the drift velocity (U^w_0) and the void fractions in the liquid slug zone and in the TB zone.

$$\Phi_{Gb}=\begin{cases}\left(U^w_0-U^{TB}_0\right)\epsilon^w_{LS}\epsilon^w_{TB} & ;U^w_0>U^{TB}_0\\ 0 & ;U^w_0\leq U^{TB}_0\end{cases} \tag{4.24}$$

The total gas entrainment for the developed slug flow is:

$$\Phi_{GS}=\epsilon^w_{TB}\left(U_{T\epsilon}-U_{GTB}\right) \tag{4.25}$$

Overall, this model was shown to account for changes in physical properties, pipe diameter and inclination, flow rates of the fluid as well as the length of the Taylor bubble.

4.1.2 Mechanistic model for non uniform film

Bendiksen et al.(1996) [40] gave the momentum equations for the TB zone as seen in Equations 4.26 and 4.27.

$$(1-\epsilon)\frac{dP_b}{dx} = -\frac{\tau_i S_i}{A} - \frac{\tau_{wb} S_b}{A} - \rho_g g\,(1-\epsilon)\sin\phi \tag{4.26}$$

$$\rho_m \frac{d}{dx}\left[(U_f - U_B)^2\,\epsilon\right] + \epsilon\frac{dp_b}{dx} + g\rho_m \cos\phi \frac{d}{dx}(\epsilon\xi) = \frac{\tau_{wf} S_f}{A} + \frac{\tau_i S_i}{A} - \epsilon g \sin\phi \cdot [\rho_l h_f + \rho_g (1 - \tag{4.27}$$

A study at IFE (2007) [41] gave the mechanistic balances for the gas and liquid phases as seen Equations 4.28 and 4.29, respectively. These equations were used to calculated the different parameters allowing for a non-uniform bubble shape in the TB zone.

$$\rho_G\,(u_{GB} - V_T)\frac{d\,(u_{GB} - V_T)}{dx} = -\frac{dp_i}{dx} + \frac{\tau_G S_G + \tau_i S_i}{A_G} - \rho_G g\left(\cos\phi\frac{dh_{LB}}{dx} - \sin\phi\right) \tag{4.28}$$

$$\rho_L\,(u_{LB} - V_T)\frac{d\,(u_{LB} - V_T)}{dx} = -\frac{dp_i}{dx} + \frac{\tau_L S_L - \tau_i S_i}{A_L} - \rho_L g\left(\cos\phi\frac{dh_{LB}}{dx} - \sin\phi\right) \tag{4.29}$$

Comparing these two sets of new mechanistic balances in the section abovenew terms are visible. The first terms in Equations 4.27 and 4.29 are the acceleration term for the liquid film relative to the translation velocity of the slug. This will allow for the liquid film to have a velocity profile that develops in the TB zone. The same acceleration term can be seen as the first term in Equation 4.28 for the gas momentum balance. The change of velocity in the film will be given by the continuity of the liquid film, meaning that the film height will change along the pipe. This can be seen in the last term on the left hand side in Equation 4.27 and as the last term in Equation 4.29.

4.1.3 Mechanistic pressure drop calculations

The pressure drop in slug flow normally to consist of the contributions from the two different zone in the slug, the TB zone and the liquid slug zone.

$$\Delta P_{tot} = \Delta P_s + \Delta P_f \tag{4.30}$$

The first term in Equation 4.30 is the pressure drop for the liquid slug unit adjusted for entrained gas, the second term is the pressure drop due to the liquid film in front of the liquid slug. The pressure drop from the gas in the Taylor bubble is normally neglected as the contribution from this this is very low compared to the pressure drop in the liquid. Due to the zone contributing differently, the slug length and the frequency of the liquid slugs will be important in the pressure drop calculations[42].

Evaluating the pressure drop for a slug unit, assuming uniform profiles in the TB zone and that the pressure drop in the liquid slug zone can be calculated as the pressure drop for bubble flow, Equation 4.30 can be written as Equation 4.31 [8].

$$\left(\frac{dP}{dx}\right)_{tot} = 2\frac{f_s}{D}\rho_s U_s^2 \frac{l_s}{l} + \frac{\tau_f S_f - \tau_i S_i}{A_f}\frac{l_f}{l} \tag{4.31}$$

Where ρ_s is the mixture density, $\rho_s = \rho_l\, H_s + \rho_g\, (1 - H_s)$ and f_s is the friction factor for a smooth pipe and turbulent flow, $f_s = 0.046/Re_s$.

$$Re_s = \frac{\rho_s U_s D}{\mu_{\text{eff}}} \tag{4.32}$$

with $\mu_{\text{eff}} = \mu_L\,(1 + 2.5\ E_s) = \mu_L\,(3.5 - 2.5\ H_s)$

Liquid film effect on pressure drop in liquid slug body

Evaluating the turbulence in the liquid slug body as determining for the bubble entrainment, Zhang et al.[25] argued that the turbulence in the liquid slug body is a product of both wall shear stresses as well as the momentum transfer between the liquid film and slug body.

$$\left(\frac{dP}{dx}\right)_{sm} = \left(\frac{dP}{dx}\right)_{s} + \left(\frac{dP}{dx}\right)_{m} \tag{4.33}$$

The pressure drop due to wall shear stress was found from Equation 4.34

$$\tau_s = \frac{f_s}{2}\rho_s U_m^2 = \left(\frac{dP}{dx}\right)_{s} \frac{d}{4} \tag{4.34}$$

The additional pressure drop in the slug body due to the momentum transfer between the liquid film and the slug body was calculated as

$$\left(\frac{dP}{dx}\right)_{m} = \frac{\rho_L H_f \left(U_t - U_f\right)\left(U_m - U_f\right)}{l_s} \tag{4.35}$$

This results in a total pressure drop in the liquid slug body of

$$\left(\frac{dP}{dx}\right)_{slug\ body} = \left(\frac{dP}{dx}\right)_{sm} = \frac{2f_s}{d}\rho_s U_m^2 + \frac{\rho_L H_f \left(U_t - U_f\right)\left(U_m - U_f\right)}{l_s} \tag{4.36}$$

Calculation of pressure and slug lengths

Bagci (2010)[42] studied how pipes consisting of several sections with different inclinations would affect the slug flow and generation of pseudo-slugs. Using a sink/source concept a mathematical computer

program was used to calculate the flow. The sink/source concept uses geometrical changes (e.g. inclination change) and specifies these based on whether they will increase the slugging or decrease it. The minimum stable slug length was evaluated as dependent of the inclination and given as follows

$$L_{s,\min} = 16D\,(1 + cos\alpha) \tag{4.37}$$

The minimum stable slug length is a parameter used to calculate the capacity of the different sink and sources. The pressure drop calculations were done neglecting the gas phase pressure drop for the slug unit, and the slug lengths were estimated using the pipe diameter.

The slug front velocity was estimated to be the mixture velocity of the slug. The liquid holdup was calculated using the fitting equations for the liquid slug holdup.When limiting size of the sink, pseudo-sinks were produced. The film holdup was found to be directly depended on the superficial liquid velocity, but also indirectly dependent on the pipe inclination. The slug length was found to increase with increasing inclination. A diameter effect on the slug length was also found and the sinks became more important with increasing diameter.

4.1.4 Turbulence

In the liquid slug body turbulence will normally be present, and this will induce large vortices, primarily over the upstream film height. Rout et al.(2002)[43] studied the velocity fluctuations behind a TB in vertical pipes by ensemble-averaging data for rising bubble in stagnant water. Turbulent fluctuation was found two diameters (2D) into the slug, but after this the turbulence was only barely present, so the flow should be considered as laminar. Turbulent vortices were also found at 30D and even at 50D into the slug. The oscillation of the

TB was found to not have an effect longer into the slug than 0.5D. The effect of the annular jet gives rise to higher velocities in the liquid slug, with a maximum at 0.06 x/D to zero at 1.8 x/D.

The turbulent dissipation has also been subject to mechanistic evaluation. Being caused by the shear between the fluids and the wall in addition to the shear stress between the phases, the power dissipation per unit mass was given by Barnea, 2013[6], as

$$\epsilon = \frac{dp}{dx}\frac{U_m}{\rho} = \tau\frac{4}{D}\frac{U_m}{\rho} = f\frac{2}{D}U_m^3 \tag{4.38}$$

Turbulent velocity fluctuations

Zhang et al. [25] used an expression for the turbulent kinetic energy per unit volume of liquid presented by White (1991)

$$e_T = \frac{1}{2}\rho_L\left(\overline{u_r'^2} + \overline{u_\theta'^2} + \overline{u_z'^2}\right) \tag{4.39}$$

For the whole liquid slug body, Equation 4.39 when assuming isotropic turbulence $\left(\overline{u_r'^2} = \overline{u_\theta'^2} = \overline{u_z'^2}\right)$ becomes

$$E_T = \frac{3}{2}\rho_L\overline{u_r'^2}AH_{Ls}l_s \tag{4.40}$$

The velocity fluctuations were approximated as the friction velocity

$$\sqrt{\overline{u_r'^2}} = u^* = \sqrt{\frac{\tau_s}{\rho_L}} \tag{4.41}$$

where the wall shear stress, τ_s is

$$\tau_s = \frac{f_s}{2}\rho_m U_m^2 = \left(\frac{dP}{dx}\right)_s \tag{4.42}$$

It was argued that since the pressure drop not only is affected by the wall shear stress but also by the momentum exchange between the liquid film jet and the slug body, that the pressure drop in Equation 4.42 should be the same as in Equation 4.36. Combining the above equations with Equation 4.36 gives the turbulent kinetic energy for the liquid slug body.

$$E_T = \frac{3}{2}\left(\frac{2f_s}{d}\rho_s U_m^2 + \frac{\rho_L H_f \left(U_t - U_f\right)\left(U_m - U_f\right)}{l_s}\right) A H_{Ls} l_s \tag{4.43}$$

4.1.5 Surface energy of dispersed bubbles

Considering the formation of the bubbles entrained in the liquid slug, attempts have been made to use the energy needed to make these bubbles to estimate the void fraction. The surface energy of the liquid slug body is the total work needed to generate the total interfacial area of the bubbles.

A study performed for Hydro Oil and Energy [44] approximated the surface energy of the dispersed bubbles in the liquid slug as

$$E_s = 4\pi r^2 \sigma n = 3\phi\frac{\sigma}{r} \tag{4.44}$$

where σ is surface tension and ϕ is void fraction. The void fraction was expressed as a function of bubble radius and number of bubbles per volume, n .

$$\phi = \frac{4}{3}\pi r^3 n \tag{4.45}$$

Zhang et al. [25] assumed all the bubbles in the slug body to be spherical with a diameter of d_b and approximated the surface energy as in Equation 4.46

$$E_s = \frac{6\sigma}{d_b} A \left(1 - H_{Ls}\right) l_s \tag{4.46}$$

4.2 Solving non-linear algebraic equations

The solving of nonlinear algebraic equations can be done using many different methods when an analytic solution is not available or hard to achieve. Some of the different methods are the bisection method, secant method, regula-falsi method and Newton's method. All these methods evaluate the equation

$$f(x) = 0$$

In other words, an equation of the form

$$f(x) = g(x)$$

has to be solved as

$$f(x) - g(x) = 0$$

The method used to solve the mechanistic model was the bisection, which is explained in the following section.

Bisection method

If a function, $f(x)$, is considered in an interval [a,b] and $f(a) \cdot f(b) < 0$, the function will have a zero value at least once in the interval. The concept of the bisection method is to divide the interval into two

sections, [a,c] and [c,b], and see in which of the new interval the product of the function evaluated at the boarders, change sign. This is repeated until wanted convergence is achieved. The residual being the size of the interval.

4.3 Data collection

Data were collected from eight different sources. The different sources are listed in Table 4.1 below. The physical parameters of the fluids and pipes used in the different experiments, see Appendix A.

Author	**Fluid system**	**Measured parameters**	**Number of points**
Gregory et al. (1978) [3]	Air - Oil	U_{sl}, U_s and H_s	62 105
Abdul-Majeed et al. (1999) [24]	Air - Heavy oil	U_{sl}, U_s and H_s	35
Nuland et al. (1997) [19]	Dense gas(SF6) - Oil	U_{sl}, U_s, U_t, H_f, Φ and H_s	20
Kouba (1986) [45]	Air - Kerosene	T, p, U_{sl}, U_{sg}, U_t, L_s, L_p, Re, ΔP_s, $\Phi$and H_s	53
Roumanzeilles (1994) [2]	Air - Kerosene	T, p, U_{sl}, U_{sg}, U_t, L_s/D, ΔP_s, Φ and H_s	103
Hout et al. (2002) [46]	Air - Water	U_{ls}, U_{gs}, U_t, U_b, U_d, Φ, l_s, l_B and H_s	12 6
Tiller data [47]	Diesel - Nitrogen gas	U_{sl}, U_s and H_s	63, 53 97

Table 4.1: Overview of different data sets

4.4 Solution of mechanistic model

The mechanistic balance, see Section 4.1, was solved using Matlab for the data sets for horizontal pipes, provided by Gregory et al. [3], Abdul-Majeed [24], Kouba [45], Roumanzeilles [2] and from the experimental facility at Tiller [47], see Table 4.1. A summary of the physical properties for the different experiments can be seen in Appendix A. The superficial velocities, physical parameters (both for the fluids and pipe) and the void fraction, H_s, were used as inputs. The bisection method was used to calculate the height of the liquid film by iterating on the θ in Equation 4.16 using Matlab.

$$H_f = \frac{\theta - 0.5\sin(2\theta)}{\pi} \tag{4.16}$$

The complete Matlab script can be seen in Appendix B.

The bisection method was set up to allow for multiple solutions of θ, as this turned out to be important in order to find the correct solution for some cases. When solving the mechanistic model for experimental data from inclined pipes, the model failed to give overall good values, as the calculated values for the length fractions were often not in the region [0,1].

4.5 Results

The solution of the mechanistic balance offers a possibility to use the local velocities in the slug when calculating the liquid holdup. This makes it possible to evaluate different kind of models, as done in the following section. In order to ensure that all the cases represent real slug flow condition, cases with reported liquid holdup equal or below 0.4 ($H_s \leq 0.4$) were excluded from the data sets. A statistical fitting

parameter, R^2, was calculated for all models, showing large variation of the predictions. See Appendix C for calculation of R^2 procedure.

4.5.1 Agreements with earlier models - Horizontal pipes

The models evaluated in this section, are the models already presented in Section 2.5.

Using the simple correlation proposed by Gregory et al., a good prediction of the liquid holdup was found. The R^2 was calculated to be 0.90, and so this model offers good prediction of the void fraction for a large range of values.

As can be seen in Figure 4.5 the prediction accuracy decreases for decreasing liquid holdups.

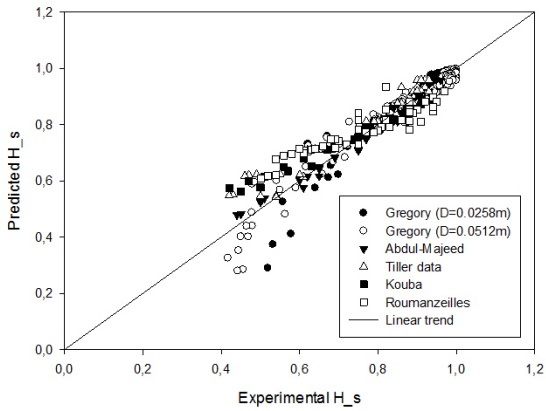

Figure 4.5: Gregory model predictions for horizontal pipes

The model tested by Nuland et al. [19], is a model intended to be used on inclined pipes. It estimates the void fraction for horizontal

and vertical pipes, and then a value for the inclination is calculated using Equation 2.14. The void fraction is set to only occur at mixture velocities above a certain onset velocity, U_{ss}, see Equation 2.16. Since this onset velocity was higher than the mixture velocity in most cases, the number of cases calculated to have a void fraction was low. As seen in Figure 4.6, prediction of the holdup was only possible for holdup values below 0.8. The parameter fitting was calculated to have an $R^2 = 0.85$.

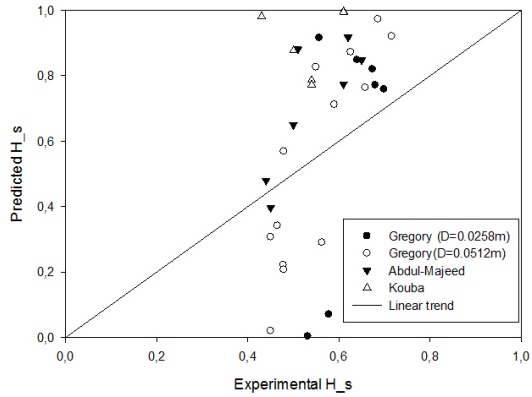

Figure 4.6: Nuland model predictions for horizontal pipes

The model of Abdul-Majeed is also based on the mixture velocity as the two previous models. This however also takes into account the viscosity of the different phases as shown in Equation 2.20. As shown in Figure 4.7 the scatter of the data is very low, but model is found to overpredict the values of liquid holdup, giving the model a $R^2 = 0.39$.

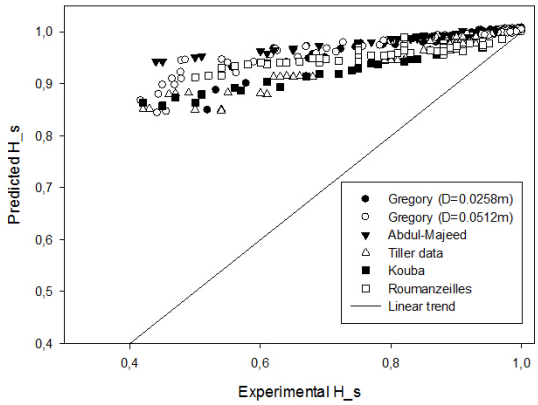

Figure 4.7: Abdul-Majeed model predictions for horizontal pipes

The energy consideration proposed by Zhang et al., offers a different approach to calculating the void fraction then the other models. For the calculations in this model, the velocities from the mechanistic balance were used in the estimation of the turbulence kinetic energy. The model predicts good for some data sets, but overpredicts for other (Kouba) as shown in Figure 4.8. The calculated R^2 was found to be 0.65 for the data set considered.

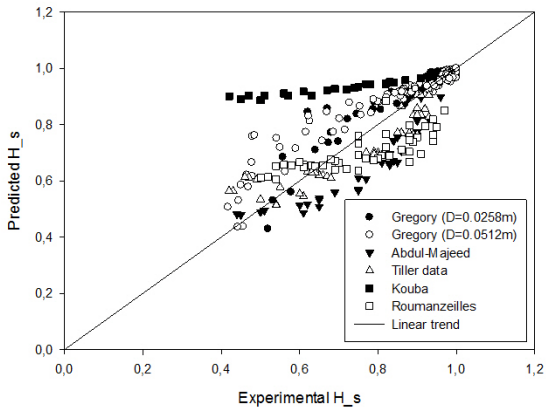

Figure 4.8: Zhang model predictions for horizontal pipes

Similarly to Zhang et al., Al-Safran used a dimensionless momentum transfer rate, θ, to estimate the liquid holdup, as shown in Equations 2.27 to 2.32. The transfer rate, θ, offers a possibility to calculate the liquid holdup without using any physical parameters, in contrast to the models of Abdul-Majeed, Nuland and Zhang. For the empirical equation given based on the data set by Al-Safran, the R^2 was found to be 0.65.

$$H_{LS} = 1.05 - \frac{0.0417}{\Theta - 0.123} \tag{2.32}$$

Using the empirical equation by Al-Safran, Equation 2.32, the predictions were found to be too low, see Figure 4.9. Due to the form of Equation 2.32, predictions for values close to 0.123 will shown asymptotic behaviour and these points were therefore excludes when calculating the R^2. The R^2 was found to be 0.66, slightly better than for the Zhang-model.

The values here show much less scattering than the values calculated with the Zhang model.

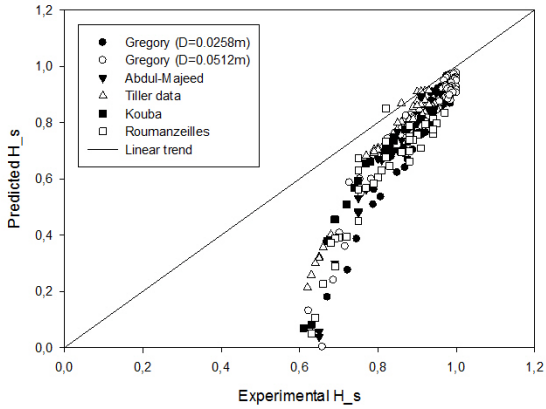

Figure 4.9: Al-Safran model for horizontal pipes

Changing empirical parameters

Since the models presented by Abdul-Majeed and Al-Safran show calculated values with little scatter, but trends shifted from the wanted linear trend, new empirical parameters were tested. This was done in order to investigate how well the equation form used in the respective models, could be expected to perform.

For Abdul-Majeed the new constant were found to as shown in Equations 4.47 and 4.48, with A the same as the in the original equation. Using these constant, the model was found to have a $R^2 = 0.86$.

$$H_{LLS} = (0.9843 - CV_M)\, A \tag{4.47}$$

where

$$C = 0.0420 + 2.4502\, \frac{\mu_G}{\mu_L} \tag{4.48}$$

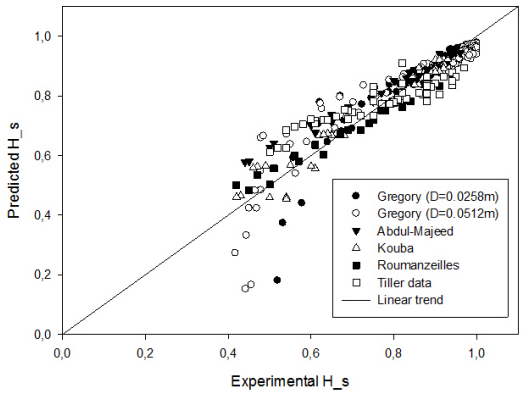

Figure 4.10: Abdul-Majeed model predictions using new constant

The empirical parameters in Equation 2.32 were also adjusted to this data set. The correlation between θ and H_s was found to be better represented by Equation 4.49, giving a R^2 of 0.95.

$$H_s = 1.0932 - \frac{0.07239}{\theta - 0.005543} \tag{4.49}$$

Equation 4.49 is drawn together with the experimental values in Figure 4.11, and the predicted values compared to the experimental values in Figure 4.12.

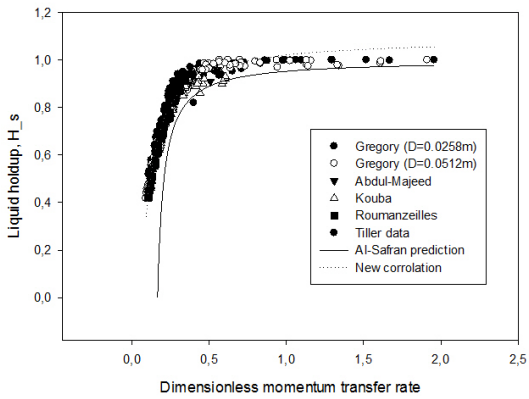

Figure 4.11: Comparison of correlation of dimensionless momentum transfer rate and liquid holdup using Al-Safran constant and new constants

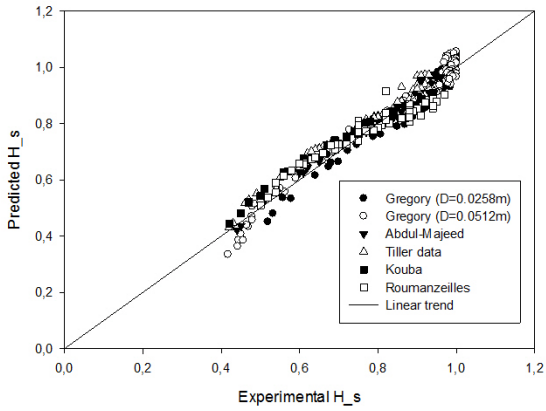

Figure 4.12: Predictions using dimensionsless momentum transfer rate and new constants

4.5.2 Agreements with earlier models - Inclined pipes

For inclined pipes, data was collected from van Hout et al. [46], Nuland et al.[19] and Tiller [47]. The Tiller data provide many data points for $0°, 1°$ and $5°$, while Nuland and Hout provide a small number of data points for $0° - 60°$ and $0° - 90°$, repsectively. The same models as for horizontal pipes were tested. To illustrate the increased difficulty in using the mechanistic balance, the amount of the usable points of the original dataset was calculated for the three different angles provided in the Tiller data.

For horizontal pipe, the all the calculate points when using the mechanistic model was usable. Inclining the pipe $1°$, four out of the 53 points gave non-physcial values. At $5°$ pipe inclination five out of the 93 got three different solution with one physical understandable value. 65 out the 97 data points got were calculated to have unphysical length fraction, and five of the points were remove due to an unphysical pressure drop.

The Gregory was found to have a stronger tendency to overpredict the holdup than when used for horizontal pipes, see Figure 4.13.

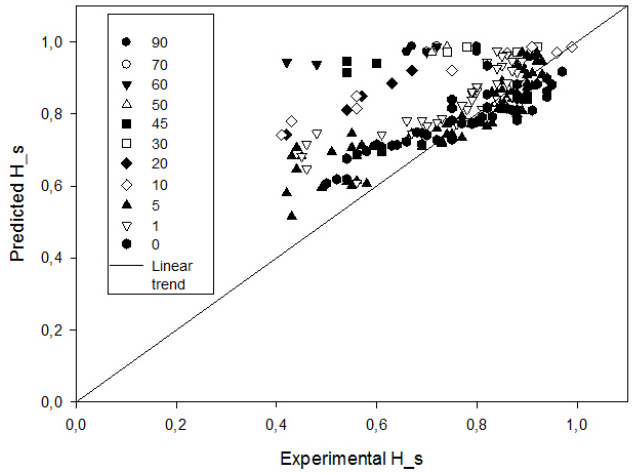

Figure 4.13: Gregory model prediction for inclined pipes

The model from Nuland et al. was able to predict the holdup for more points than for horizontal pipes. The predicted values were mostly underpredicted as can be seen in Figure 4.14.

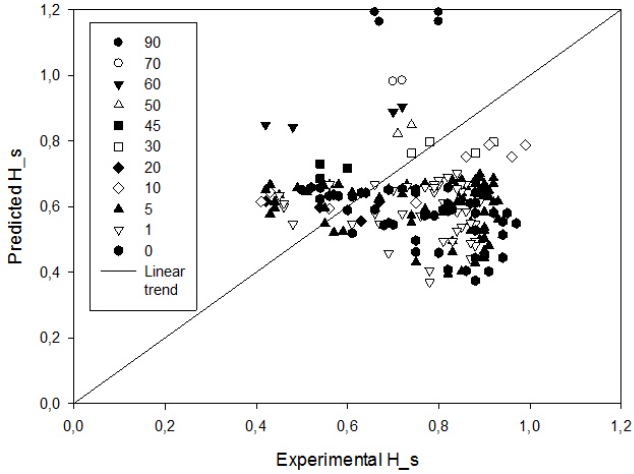

Figure 4.14: Nuland model predictions for inclined pipes

The model of Abdul-Majeed was found to estimated the hold slightly better for 5° than for horizontal pipe. The values for higher angles showed a large scatter for the predicted liquid holdup versus the experimental holdup, as shown in Figure 4.15.

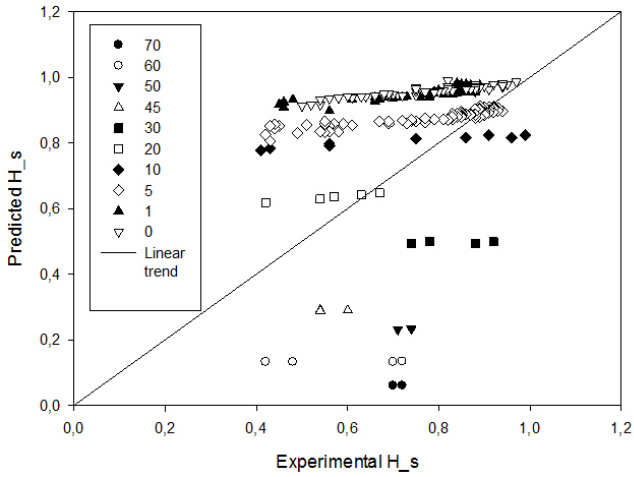

Figure 4.15: Abdul-Majeed model predictions for inclined pipes (using old constants)

For the models of Al-Safran and Zhang, the velocities calculated from the mechanistic model are needed. As the mechanistic model does not take pipe inclination into account, only the values with physically reasonable values for length fractions and pressure drop were considered. The calculation based on the model of Zhang includes a factor taking in the pipe inclination. The model showed a large scatter for the different angles, see Figure 4.16.

As the empirical correlation in Equation 2.32 did not show a satisfying fit for horizontal pipes, it was not tested for inclined pipes. Instead the correlation between the dimensionless momentum transfer rate and the liquid holdup is shown in Figure 4.17.

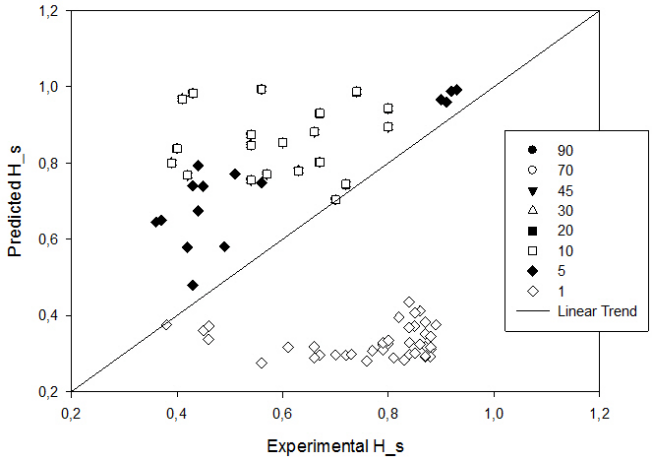

Figure 4.16: Zhang model predictions for inclined pipes

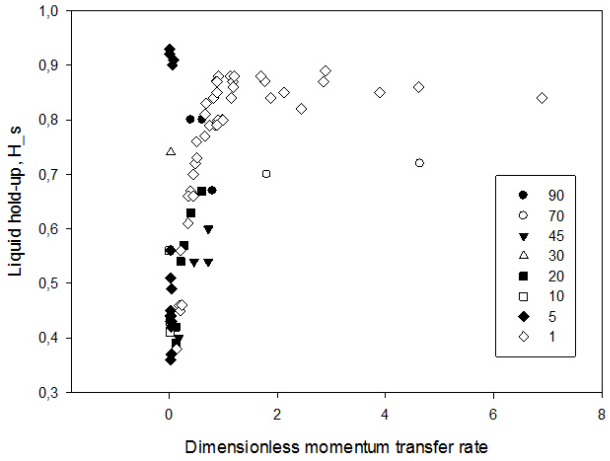

Figure 4.17: Dimensionless momentum transfer rate versus liquid holdup for inclined pipes

4.6 Summary and discussion

Solving of the mechanistic balance makes it possible to study models predicting liquid holdup in slugs using local velocity parameters. For horizontal pipes, the model predicted reliable values, while for inclined pipes it was detected some difficulties for calculation of good values. The mechanistic balance made i possible to study the momentum transfer between the liquid film and the slug, and a simple correlation using the dimensionless momentum transfer rate was found to predict the liquid hold with an R^2, the best among the models tested.

The model of Zhang et al., includes the momentum exchange between the liquid film and the slug body as one of multiple affecting parameters. This was not found to increase the accuracy of the predictions, as the calculated $R^2 = 0.65$. The best estimation of the liquid holdup was found to be based on a dimensionless momentum transfer rate, representing the momentum transfer between the liquid film and the liquid slug body.

Solving the mechanistic model for inclined pipes did not give the same type of quality results as for horizontal pipes. Explanations for this is thought to be the lack of satisfying assumptions. The liquid film in a inclined pipe has the possibility to have an non-uniform velocity distribution the Taylor bubble, which is assumed to have an effect on the calculated result.

Part 5

Conclusion

The gas entrainment at a slug front was studied using a transient 2D channel CFD simulation in the commercial CFD package StarCCM+. The simulation was set up with a reference frame moving with the propagating velocity of the Taylor bubble. A sectioning of the domain was done using a velocity recirculation rate, and void fractions were reported for both the wake zone and the developed slug body.

The liquid film velocity, the bubble propagation velocity, the pipe inclination and the liquid film height were all found to affect the momentum transfer between the liquid film and the slug body, thus also affecting the gas entrainment rate. The results show that the gas entrainment at the slug front will be related to the shear between the slug front and the liquid film. The recirculation in the slug body will contribute to different void fractions in the wake zone and in the developed slug body. The turbulent kinetic energy in the flow was used to study the interaction between the film and the slug body. Changing different parameters, revealed that multiple parameters are affecting the interaction, and that quantifying the momentum transfer between the liquid film and the liquid slug body with the turbulence kinetic energy can be used as a way to study the gas entrainment

and void fraction in a slug.

Following the results from the simulation, a model prediction for the liquid holdup in the slug using the momentum exchange between the liquid film and the slug body at the slug front was sought. Two different models using a momentum exchange consideration were tested and compared to other, more simple models. In order to use these models, a mechanistic balance had to be solved. The mechanistic balance gave good results for horizontal pipes, but improvement of the model before applying it to inclined pipes is considered necessary. The results from solving data from inclined pipes using the simple mechanistic model had a large amount of points being calculated with unphysical values.

The best model was found to be the one using a dimensionless momentum transfer rate between the liquid film and the liquid slug body. This model gave very good predictions of the liquid holdup with an $R^2 = 0.95$.

Both the results from the simulations and the solving of the mechanistic balance documented that considering the momentum transfer at the slug front may be useful when predicting the liquid holdup in slugs.

Bibliography

[1] M.K. Abdullahi. *Slug front gas entrainment in gas-liquid two-phase flow in horizontal and near horizontal pipes*. PhD thesis, Imperial College London, 2013.

[2] P. Roumanzeilles. *An experimental study of downward slug flow in inclined pipes*. PhD thesis, University of Tulsa, 1994.

[3] G.A. Gregory, M.K. Nicholson, and K. Aziz. Correlation of the liquid volume fraction in the slug for horizontal gas-liquid slug flow. *International Journal of Multiphase Flow*, 4, 1978.

[4] M. Nädler and D. Mewes. Effects of the liquid viscosity on the phase distributions in horizontal gas-liquid slug flow. *International Journal of Multiphase Flow*, 21(2), 1995.

[5] X. Wang, T. Wang, and L. He. Measurment of gas entrainment from stationary liquid slug in horizontal tube with double-sensor conductivity probe. *Flow Measurement and Instrumentation*, (27), 2012.

[6] D. Barnea, E. Roitberg, and L. Shemer. Spatial distribution of void fraction in the liquid slug in the whole range of pipe inclinations. *International Journal of Multiphase Flow*, (52), 2013.

[7] Y. Taitel and D. Barnea. A consisten approach for calculating pressure drop in inclined slug flow. *Chemical Engineering Science*, 45(5), 1990.

[8] A. Orell. Experimental validation of a simple model for gas.liquid slug flow in horizontal pipes. *Chemical Engineering Science*, 60, 2005.

[9] M.N. Kashid et al. Prediction of slug liquid holdup in horizontal pipes. *Journal of Energy Resources Technology*, 131, 2009.

[10] N. Brauner and A. Ullmann. Modelling of gas entrainment from taylor bubbles. part a: Slu flow. *International Journal of Multiphase Flow*, (30), 2004.

[11] K. Yan and D. Che. Hydrodynamic and mass transfer characteristics of slug flow in a vertical pipe with and without dispersed small bubbles. *International Journal of Multiphase Flow*, 37, 2011.

[12] T. Höhne. Experiments and numerical simulations of horizontal two phase flow regimes. *Seventh International Conference on CFD in the Minerals and Process Industries*, 9-11 December 2009.

[13] S. Mo, A. Ashrafian, J.-C. Barbier, and S.T. Johansen. Quasi-3d modelloing of two-phase slug flow in pipes. *9th international Conference on CFD in the Minerals and Process Industries,*, 2012.

[14] J. Fabre. *Gas-liquid slug flow*, 2002. Modelling and Control of Two-Phase Flow Phenomena, International Centre for Mechanical Sciences, Udine, Italy.

[15] D.M. Holland, R.R. Rosales, D. Stefanica, and E.G. Tabak. Internal hydraulic jumps and mixing in two-layer flows. *Journal of Fluid Mechanics*, 470, 2002.

[16] J.R. Fagundes Netto, J. Fabre, and L. Peresson. Shape of long bubbles in horizontal slug flow. *International Journal of Multiphase Flow*, (25), 1999.

[17] H. Tennekes and J.L. Lumley. *A First Course in Turbulence*. The MIT press, 1972.

[18] H. Wengle. Lecture notes in numerical calculation of turbulent flows. at TUM, Germany, 2011 - 2012.

[19] S. Nuland, I.M. Malvik, A. Valle, and P. Hedne. Gas fractions in slugs in dense-gas two-phase flow from horizontal to 60 degress of inclination. The 1997 ASME Fluids Engineering Division Summer Meeting, June 22-26 1997.

[20] P. Andreussi and K. Bendiksen. An investigation of void fraction in liquid slugs for horizontal and inclined gas-liquid pipe flow. *Internation Journal of Multiphase Flow*, 15(6), 1989.

[21] E.M. Abed and R.S. Al-Turaihi. Experimental investigation of twp-phase gas-liquid slug flow inclined pipe. *Journal of Babylon University/Engineering Sciences*, 21(5), 2013.

[22] T. Taha and Z.F. Cui. CFD modelling of slug flow in vertical tubes. *Chemical Engineering Science*, 617, 2006.

[23] R. Skartlien et al. A gas entrainment model for hydraulic jumps in near horizontal pipes. *International Journal of Multiphase Flow*, 43, 2012.

[24] G.H. Abdul-Majeed. Liquid slug holdup in horizontal and slightly inclined two-phase slug flow. *Journal of Petroleum Science and Engineering*, 27, 2000.

[25] H.-Q. Zhang, Q. Wang, C. Sarica, and J.P. Brill. A unified mechanistic model for slug liquid holdup and transition between slug and deispersed bubble flows. *International Journal of Multiphase Flow*, 29, 2003.

[26] F.M. White. *Viscous Fluid Flow.* McGraw-Hill , 3rd edition, 2006.

[27] B.A. Nichita, I. Zun, and J. Thome. A level set method coupled with a volume of fluid method for modelling of has-liquid interface in bubbly flow. *Journal of Fluid Engineering*, 132, 2010.

[28] R.T. Eiswirth, H.J. Bart, T. Atmakidis, and E.Y. Kenig. Experimental and numerical investigation of a free rising droplet. *Chemical Engineering and Processing*, 50, 2011.

[29] M.R. Ansari and M.E. Nimvari. Bubble viscosity effect on internal circulation within the bubble rising due to bouyancy using the level set method. *Annals of Nuclear Energy*, 38, 2011.

[30] I. Roghair et al. On the drag force of bubbles in bubble swarms at intermediate and high Reynolds numbers. *Chemical Engineering Science*, 2011.

[31] C.W. Hirt and B.D. Nichols. Volume of fluid (vof) method for the dynamics of free boundaries. *Journal of Computational Physics*, 39, 1981.

[32] M. Darwish and F. Moukalled. Convective schemes for capturing interfaces of free-surface flow on unstructured grids. *American University of Beirut, Faculty of Engineering and Architecture, Mechanical Engineering Dept., Lebanon.*

[33] Q. Dijkhuizen, M. van Sint Annaland, and J. Kuipers. Direct numerical simulation of the drag force in bubble swarms. 6th International Conference on Multiphase Flow, ICMF, July 2007.

[34] I.W.M. Pothof and F.H.L.R. Clemens. On the modeling of gas diffusion by turbulence in hydraulic jumps. 33rd IAHR Congress: Water Engineering for s Sustainable Environment, 2009.

[35] T. Frank. Numerical simulation of slug flow regime for an air-water two-phase flow in horizontal pipes. *The 11th Interna-*

tional Topical Meeting on Nuclear Reactor Thermal-Hydraulics, 2-6 October 2005.

[36] R.I. Issa and M.H.W. Kempfl. Simulation of slug flow in horizontale and nearly horizontal pipes with the two-fluid models. *International Journal of Multiphase Flow*, (29), 2003.

[37] M. Bonizzi and R.I. Issa. A model for simulationg gas bubble entrainment on two-phase horizontal slug flow. *International Journal of Multiphase Flow*, (29), 2003.

[38] J. Hua, J. Nordbø, and M. Foss. CFD modelling of gas entrainment at a propagating slug front. 10th International Conference on CFD in Oil & Gas, Metallurgical and Process Industries, 17-19 June 2014.

[39] N. Brauner and A. Ullmann. Modelling of gas entrainment from taylor bubbles. part a: Slug flow. *International Journal of Multiphase Flow*, 40, 2004.

[40] K.H. Bendiksen, D. Malnes, and O.J. Nydal. On the modelling of slug flow. *Chem. Eng. Comm.*, 141-142, 1996.

[41] B. Hu. *A new slug flow popint model including the tail-profile in the slug bubble region*, 2007. IFE/KR/F - 2007/140.

[42] S. Bagci. An investigation of two-phase slug flow in inclined pipelines. *Energy Sources*, 26(7), 2010.

[43] R. van Hout, A. Gulitski, D. Barnea, and L. Shemer. Experimental investigation of the velocity field induced by a Taylor bubble rising in stagnant water. *International Journal of Multiphase Flow*, 28, 2002.

[44] R. Schulkes. *Gas entrainment at a propagating slug front*. Hydro Oil & Energy.

[45] G.E. Kouba. *Horizontal slug flow modeling and metering*. PhD thesis, University of Tulsa, 1986.

[46] R. van Hout, D. Barnea, and L. Shemer. Translational velocities of elongated bubbles in contiuous slug flow. *International Journal of Multiphase Flow*, 28, 2002.

[47] P. Andersson. *Reanalysis of Tiller data (1984-1986) with special attention to void in slug data*, 2007. IFE/KR/F - 2007/033.

Appendix A

Overview over fluid properties

Table A.1: Fluid properties for different experiments

Experiments	**Fluids**	**Liquid density [kg/m^3]**	**Liquid viscosity [Pa s]**	**Gas density [kg/m^3]**	**Gas viscosity [Pa s]**	**Interfacial tension [N/m]**	**Diameter [m]**
Gregory et al.	light oil - air	858	$6.754 \cdot 10^{-3}$	1.1925	$1.83 \cdot 10^{-5}$	N/A	0.0258 0.0512
Nuland et al.	Dense gas(SF6) - Oil	820	$1.8 \cdot 10^{-3}$	47	$1.5 \cdot 10^{-5}$	$20.7 \cdot 10^{-3}$	0.0762
Abdul-Majeed	Air - Heavy oil	960	$20 \cdot 10^{-3}$	1.1925	$1.83 \cdot 10^{-5}$	N/A	0.0512
Roumanzeilles	Air - Kerosene	800	$1.64 \cdot 10^{-3}$	1.1925	$1.83 \cdot 10^{-5}$	0.029	0.0762
Kouba	Air - Kerosene	800	$1.64 \cdot 10^{-3}$	1.1925	$1.83 \cdot 10^{-5}$	0.029	0.0762
Rout et al.	Water - air	998	0.001002	1.1925	$1.8348 \cdot 10^{-5}$	0.002	0.0240 0.0540
Tiller data	Diesel - Nitrogen gas	825.5	0.00264	22.4	$1.81 \cdot 10^{-5}$	0.00231	0.19

Appendix B

Matlab scripts

B.1 Main file

```
clear all
format long

%Global constants
global g rho_g Cf Cg m visc_g f_i rho_l visc_l sigma

g = 9.81;
Cf = 0.046;
Cg= 0.046;
m = 0.2 ;
f_i = 0.0142 ;

margin = 10e-6;
k=1;

%Input data set
[U_sl, U_sg, H_s, Dia, Phi_ex,
        rho_l, visc_l, rho_g, visc_g, sigma] =Gregory_0258;
```

```
U_m = U_sl + U_sg;

for i = 1:length(U_sl)

Usl = U_sl(i);
Usg = U_sg(i);
Hs = H_s(i) ;
Phi =Phi_ex(i);
D = Dia(i) ;

%Calculation of film height
theta = test_theta2(Usl, Usg, Hs, D, Phi);

    for j = 1:length(theta)
      a = j+b;
    Th = theta(j);

    [Uf, Hf, Ug , Ut, dP, Residual, ls_frac]
                =  calc_bisec(Usl, Usg, Hs, Th, D, Phi);

    U_f(a) = Uf;
    H_f(a) = Hf;
    U_g(a) = Ug;
    U_t(a) = Ut;
    f_s_frac(a) = ls_frac;
    vink(a,:) = Th;
    dPdx_t(a) = dP;
    Dia2(a) = Dia(i);
    U_sl2(a) = U_sl(i);
    U_sg2(a) = U_sg(i);
    H_s2(a) = H_s(i);
    U_m2(a, :) = U_m(i);
    No(a,:) = i;
    Phi2(a,:) = Phi_ex(i);
    end
    b = length(U_sl2);
end

fprintf('Uf, Hf, Ug, Ut, vink,
                Hs, D, Um, i , dPdx, Ur, Mom_theta')
Data = [U_f', H_f', U_g', U_t', vink, H_s2', Dia2', U_m2, No];
```

```
dPdx_temp =dPdx(H_s2', U_m2(:,1), Dia2', dPdx_t', f_s_frac');
dPdx_2  =dPdx_2(H_s2', U_m2(:,1), Dia2', dPdx_t', f_s_frac',
                                  U_t', U_f', H_f', Phi2);

Data = [Data, dPdx_temp];

%Relative velocity
U_r = U_t' - U_f';
Data = [Data, U_r];

%Calculation of the dimesionsless momentum transfer rate.
Mom_theta = (H_f'.*(U_t' - U_f').*(U_m2-U_f'))./(U_m2.^2);



for i = 1: length(U_m2)
   Hs_Zhang = Zhang(U_m2(i), Phi2(i), Dia2(i),  U_f(i), H_f(i), U_t(i))
   Hs_Zhang2(i) = Hs_Zhang;
end

%Estimations using Zhang model
Data_Zhang = [Data_excel, Hs_Zhang2'];

%Plotting of the results

figure(1)
hold on
title('Hs vs Theta for calculated values of Theta')
scatter(Data(:,12), Data(:,6), 's')
set(gca, 'XScale', 'log')
xlabel('Momentum transfer rate')
ylabel('Hs')
hold off

figure(2)
hold on
scatter(Data(:,11),Data(:,6))
xlabel('Ur') % x-axis label
ylabel('Hs') % y-axis label
hold off
```

```
figure(3)
hold on
title('Hs vs dPdx')
scatter(Data(:,10), Data(:,6),'d')
scatter(dPdx_2, Data(:,6))
xlabel('dPdx')
ylabel('Hs')
hold off

figure(4)
hold on
title('Theta by Usl')
scatter(Theta_2, Data(:,6),'d')
hold off
return

figure(5)
hold on
scatter(Re_s, Data(:,6))
xlabel('Re')
hold off

figure(7)
hold on
scatter(U_sl2, H_s2)
xlabel('Hs')
ylabel('Usl')
hold off

figure(8)
hold on
scatter(U_sl2, U_f)
xlabel('Usl')
ylabel('U_f')
```

B.2 Allowing for multiple solutions

```
function[T_4] = test_theta2(Usl, Usg, Hs, D, Phi)

T_int = [ 0.1, 0.39, 0.68, 0.97, 1.26, 1.55, 1.84, 2.13, 2.42, 2.71, 3]
    k=1;
    test= 0;
for i = 1:length(T_int)-1
    x1 = T_int(i);
    x2 = T_int(i+1);

    Residual1 = calc_bisec2(Usl, Usg, Hs, x1, D, Phi);
    Residual2 = calc_bisec2(Usl, Usg, Hs, x2, D, Phi);

    frac = Residual1*Residual2;

    if sign(frac) < 0
        for j = 1:50
            test = 1 ;
            x3 = (x1+x2)/2;
            Residual3 = calc_bisec2(Usl, Usg, Hs, x3, D, Phi);
            if sign(Residual1 * Residual3) < 0
                x2 = x3;
            else
                x1 = x3;
            end
            if j == 50
                T_4(k) = x3
                k = k+1;
            end
        end
    end
end
    if test == 0 ;
        fprintf('No solution found')
        return
    end
```

B.3 Solving of mechanistic balance for possible solutions

```
function[Residual] = calc_bisec2(Usl, Usg, Hs, Theta, D, Phi)

global g rho_l rho_g Cf Cg m visc_g visc_l f_i ls_frac lb_frac

Hf = (Theta -0.5*sin(2*Theta))/pi;
Af = D^2/4 * (Theta-0.5*sin(2*Theta));
Ag = D^2/4 *(pi - Theta + 0.5 * sin(2*Theta));
Sf = D * Theta;
Si = D* sin(Theta);
Sg = D * (pi - Theta);
Dhf = 4*Af/Sf;
Dhg = 4*Ag/(Si+Sg);

Um = Usl + Usg;
Us = Um;
Ud = 0.54*cos(Phi)*sqrt(g*D) + 0.35 *sin(Phi) * sqrt(g*D);
Ut = 1.2 * Um + Ud;
Uf = Ut -(Hs/Hf)*(Ut-Us);

ls_frac = (Usl - Uf*Hf)/(Us*Hs - Uf*Hf);
lb_frac = 1- ls_frac;
Ug= (Usg - Us*(1-Hs)*ls_frac)/((1-Hf)*lb_frac);

f_f = Cf/((rho_l*abs(Uf)*Dhf/visc_l)^m);
f_g = Cg/((rho_g*abs(Ug)*Dhg/visc_g)^m);

Tf = 0.5 *f_f*rho_l*abs(Uf)*Uf;
Tg = 0.5 *f_g*rho_g*abs(Ug)*Ug;
Ti = 0.5 *f_i*rho_g*abs(Ug-Uf)*(Ug-Uf);

LHS = (Tf*Sf - Ti*Si)/Af + rho_l * sin(Phi);
RHS = (Tg*Sg + Ti*Si)/Ag  + rho_g * sin(Phi);
Residual = LHS - RHS;

end
```

B.4 Solving of the mechanisitc balance

```
function[Uf, Hf, Ug , Ut, dP, Residual, ls_frac] =
            calc_bisec(Usl, Usg, Hs, Theta, D, Phi)

global g rho_l rho_g Cf Cg m visc_g visc_l f_i

Hf = (Theta -0.5*sin(2*Theta))/pi;
Af = D^2/4 * (Theta-0.5*sin(2*Theta));
Ag = D^2/4 *(pi - Theta + 0.5 * sin(2*Theta));
Sf = D * Theta;
Si = D* sin(Theta);
Sg = D * (pi - Theta);
Dhf = 4*Af/Sf;
Dhg = 4*Ag/(Si+Sg);
Um = Usl + Usg;
Us = Um;
Ud = 0.54*cos(Phi)*sqrt(g*D) + 0.35 *sin(Phi) * sqrt(g*D);
Ut = 1.2 * Um +  Ud;
Uf = Ut -(Hs/Hf)*(Ut-Us);

ls_frac = (Usl - Uf*Hf)/(Us*Hs - Uf*Hf);
lb_frac = 1- ls_frac;
Ug= (Usg - Us*(1-Hs)*ls_frac)/((1-Hf)*lb_frac);

f_f = Cf/((rho_l*abs(Uf)*Dhf/visc_l)^m);
f_g = Cg/((rho_g*abs(Ug)*Dhg/visc_g)^m);

Tf = 0.5 *f_f*rho_l*abs(Uf)*Uf;
Tg = 0.5 *f_g*rho_g*abs(Ug)*Ug;
Ti = 0.5 *f_i*rho_g*abs(Ug-Uf)*(Ug-Uf);

dP= (Tf*Sf - Ti*Si)/Af + rho_l * sin(Phi);

LHS = (Tf*Sf - Ti*Si)/Af + rho_l * sin(Phi);
RHS = (Tg*Sg + Ti*Si)/Ag  + rho_g * sin(Phi);
Residual = LHS - RHS;

end
```

B.5 Liquid holdup estimations using Zhang-model

```
function[Hs_Zhang] = Zhang(U_m, Phi, D,  U_f, H_f, U_t)

%rho_l = 858; % kg/m3
%visc_l = 0.00675; % Pa/s
%rho_g = 1.1925;
%visc_g = 0.0000183;
%sigma = 0.02;
%g = 9.81;

global rho_l visc_l rho_g  sigma g %visc_g

k= 0;

eps = 0.0001;

Hs_Greg  = 1 / (1+(U_m/8.66)^1.39);


Ce = (2.5- abs(sin(Phi)))/2;
ls = (32 * (cos(Phi))^2 + 16*(sin(Phi))^2)*D;
marg = 1 + eps;
frac = 2;
while frac > marg
rho_s = Hs_Greg *rho_l + (1-Hs_Greg)*rho_g;

f_s = 1/(rho_s*D*U_m/visc_l);

en = 1/Ce;
to = f_s/2 *rho_s*U_m^2;
tre = (D/4)*(rho_s*H_f*(U_t - U_f)*(U_m-U_f))/ls;

T_sm = en * (to+tre);

nev = 3.16 *(3.16*(rho_l-rho_g)*g*sigma)^(1/2);
```

```
Hs_Zhang = 1/(1+T_sm/nev);

frac = Hs_Zhang/Hs_Greg;
k = k+1;
if frac >marg
    Hs_Greg = Hs_Zhang;
end

if k > 100
    Hs_Zhang = 1;
    return
end

end
```

Appendix C

Regression analysis

In order to evaluate how well a regression models predict values compared to experimental values, a coefficient of variation, R^2, can be calculated [9]. The R^2 uses the residual errors to evaluate how much of the variation of the calculated values are explained by the variation of the input values. For each calculated point, the residual error is calculated.

$$\epsilon_i = y_i - \hat{y}_i \tag{C.1}$$

All residuals are squared and sum together, giving the Sum of squares for residual errors, SSE.

$$\text{SSE} = \sum_{i=1}^{n} (\epsilon_i)^2 = \sum_{i=1}^{n} (y_i - \hat{y}_i)^2 \tag{C.2}$$

The Sum of squares of regression, SSR, is than calculated as the squared deviations between the calculated value and the mean value, $\tilde{y}$.

$$\mathrm{SSR} = \sum_{i=1}^{n} \left(y_i - \tilde{y}_i\right)^2 \tag{C.3}$$

The sum of the SSE and the SSR is called the total sum of squares.

$$\mathrm{SST} = \mathrm{SSE} + \mathrm{SSR} \tag{C.4}$$

The coefficient of variation is calculated as the ratio of SSR to SST.

$$R^2 = \frac{\mathrm{SSR}}{\mathrm{SST}} \tag{C.5}$$